Journal of Catalysis **187,** 59–76 (1999)
Article ID jcat.1999.2581, available online at http://www.idealibrary.com on IDEAL®

The Performances and Characterization of BaO- and BaX_2 (X = F, Cl, and Br)-Promoted Y_2O_3 Catalysts for the Selective Oxidation of Ethane to Ethene

H. X. Dai, Y. W. Liu, C. F. Ng, and C. T. Au[1]

Chemistry Department and Center for Surface Analysis and Research, Hong Kong Baptist University, Kowloon Tong, Hong Kong, China

Received January 20, 1999; revised May 26, 1999; accepted May 26, 1999

The 30 mol% MO (M = Mg, Ca, Sr, Ba)-, 30 mol% $BaCO_3$-, and 30 mol% BaX_2 (X = F, Cl, and Br)-promoted Y_2O_3 catalysts have been investigated for the oxidative dehydrogenation of ethane reaction. Adding BaO or BaX_2 to Y_2O_3 could significantly enhance the C_2H_4 selectivity. We also found that the doping of BaX_2 into Y_2O_3 could considerably reduce C_2H_4 deep oxidation. Among these catalysts, 30 mol% $BaCl_2/Y_2O_3$ performed the best. It was stable within a reaction period of 40 h, giving a C_2H_6 conversion, a C_2H_4 selectivity, and a corresponding C_2H_4 yield of ca. 72, 74, and 53%, respectively, at 640°C and 6000 mL h^{-1} g^{-1} space velocity. X-ray photoelectron spectroscopy and chemical analysis of halides indicated that the Cl^- ions were uniformly distributed in 30 mol% $BaCl_2/Y_2O_3$ whereas the halide ions in 30 mol% BaF_2/Y_2O_3 and 30 mol% $BaBr_2/Y_2O_3$ were not. With the increase of space velocity, the C_2H_6 conversion decreased and the C_2H_4 selectivity increased at 640°C over the 30 mol% $BaCl_2/Y_2O_3$ catalyst. We observed that Cl leaching was not significant in 30 mol% $BaCl_2/Y_2O_3$. However, gradual Br leaching was observed over 30 mol% $BaBr_2/Y_2O_3$. X-ray powder diffraction and CO_2 temperature-programmed desorption (CO_2-TPD) results demonstrated that the 30 mol% $BaCl_2/Y_2O_3$ catalyst is durable and is resistant to CO_2 poisoning whereas the 30 mol% BaO/Y_2O_3 and BaX_2 (X = F and Br)/Y_2O_3 catalysts are readily poisoned by CO_2 due to $BaCO_3$ formation. O_2-TPD studies showed that the addition of BaO (or BaX_2) to Y_2O_3 could obviously enhance the adsorption of oxygen molecules. We consider that such enhancement is closely associated with the defects generated due to ionic exchanges between the BaO (or BaX_2) and the Y_2O_3 phases. Among the three 30 mol% BaX_2/Y_2O_3 catalysts calcined at 900°C, 30 mol% $BaCl_2/Y_2O_3$ showed a cubic Y_2O_3 lattice most significantly enlarged and a BaX_2 lattice most pronouncedly contracted. *In situ* laser raman results indicated that there were dioxygen adspecies such as O_2^{2-}, O_2^{n-} ($1 < n < 2$), O_2^-, and $O_2^{\delta-}$ ($0 < \delta < 1$) on the 30 mol% BaO/Y_2O_3 and 30 mol% BaX_2/Y_2O_3 catalysts. Electron paramagnetic resonance results indicated that there were monoxygen O^- and dioxygen O_2^- species on Y_2O_3, 30 mol% BaO/Y_2O_3, and 30 mol% BaX_2/Y_2O_3. We suggest that the O_2^- O_2^{n-}, $O_2^{\delta-}$, and O_2^{2-} species participate in the selective oxidation of ethane to ethene whereas the O^- species were responsible for the deep oxidation of ethane.

[1] To whom correspondence should be addressed. E-mail: pctau@hkbu.edu.hk.

Key Words: **yttrium oxide; barium oxide and barium halide promoters; ethane selective oxidation; ODE reaction; ethene generation; CO_2 poisoning, active oxygen species; Raman and EPR characterization.**

INTRODUCTION

To make better use of energy resources, the catalytic conversion of light alkanes to the respective alkenes or alkynes is of significance. Ethane is the second largest constituent in natural gas and is a dominant product of the oxidative coupling of methane (OCM) reaction. Hence, the oxidative dehydrogenation of ethane (ODE) to ethene has been studied for the use of natural gas. In the past years, work has been focused on the ODE reaction over catalysts such as Li/MgO (1–4), Mo-V-Nb-O (5, 6), Mo-V-M-O (M = Ti, Cr, Mn, Fe, Co, Ni, Nb, Ta, and Ce) (7), M-V or Mo/SiO_2 (M = Li, Na, K, Rb, and Cs) (8, 9), M-ZSM-5 (M = Nb, V, Co, and Cu) (10), V_2O_5/α-TiP (11), rare earth oxides (12, 13), Na/CeO_2 (14), LaF_3/CeO_2 (15), $La_{1-x}Sr_xFeO_{3-\delta}$ ($0 \le x \le 1$) (16), layered complex metal chloride $KSr_2Bi_3O_4Cl_6$ (17), etc. Among the good ones are Mo-V-Nb-O (7) and Dy_2O_3/Li^+-MgO-Cl^- (4); ethene yield was ca. 38% at 350°C over the former and ca. 57% at 570°C over the latter.

It has been shown that chlorine or chlorine-containing compounds have promotional effects on the OCM and ODE reactions. The presence of chloride ions in the catalyst could prevent CO_2 poisoning and lower the reactivity of adsorbed oxygen (2). The activation of gaseous oxygen molecules has been generally accepted as a key step for the ODE reaction. Obviously, the nature and distribution of surface oxygen adspecies have direct effects on the catalytic behavior. Wang and Lunsford (18) detected O^-, O_2^-, and O_3^- when Li/MgO was quenched from 650°C to −196°C in liquid O_2. They suggested that in the catalytic oxidation of alkane to alkene O^- is responsible for the high alkene yield. Previously, we characterized a number of Ln-Ba-X (Ln = La, Ho, and Y; X = F, Cl, and Br) (19–22) catalysts for the OCM or ODE reaction and suggested that oxygen

0021-9517/99 $30.00

species such as O_2^-, $O_2^{n-}(1 < n < 2)$, O_2^{2-}, and $O_2^{\delta-}(0 < \delta < 1)$ might participate in the selective oxidation of ethane to ethene. The formation of these dioxygen and monoxygen adspecies on these BaX_2-modified rare earth oxide catalysts could be associated with the defect natures of the catalysts. Adding BaX_2 to Ln_2O_3 could enhance significantly the ethane conversion and ethene selectivity, but halogen leaching is a general phenomenon. We have been looking for a good combination for the halide-promoted rare earth oxide catalyst so as to lighten the leaching problem. In the present study, we report that $BaCl_2$ and Y_2O_3 is a good combination. To identify the active oxygen adspecies for ethene formation, we used *in situ* laser Raman and electron paramagnetic resonance (EPR) as well as the temperature-programmed desorption (TPD) and temperature-programmed reduction (TPR) techniques to characterize the yttrium oxide catalysts that had been modified by alkaline earth oxide or barium halides.

EXPERIMENTAL

The MO/Y_2O_3 (M = Mg, Ca, Sr, and Ba), BaX_2/Y_2O_3 (X = F, Cl, and Br), and 30 mol% $BaCO_3/Y_2O_3$ catalysts were prepared by wet-impregnation of Y_2O_3 powder, respectively, with aqueous solutions of $M(NO_3)_2$, BaX_2, and $BaCO_3$ at the desired molar ratios, followed by evaporation. The resulted pastes were dried at 120°C overnight and calcined (6 h) at 900°C (700°C for $BaCO_3/Y_2O_3$) and then in turn ground, pressed, crushed, and sieved into 40–80 mesh. To examine the influence of calcination temperature on the properties of the catalysts, we prepared catalysts that had been calcined at 800 and 1000°C as well.

The catalytic performance was tested with 0.5 g of the catalyst in a fixed-bed quartz microreactor (i.d. = 4 mm) at atmospheric pressure using a gaseous mixture of ethane (14.8 mL min^{-1}) and air (35.2 mL min^{-1}), corresponding to an ethane to oxygen molar ratio of 2/1 and a space velocity of 6000 mL h^{-1} g^{-1}. A thermocouple was placed in the middle of the catalyst bed to determine the reaction temperature. The product mixture (C_2H_6, C_2H_4, CH_4, CO, CO_2, and O_2) were analyzed on line by a Shimadzu 8A TCD gas chromatography with Porapak Q and 5A molecular sieve columns. For the variation of space velocity (SV), the reactant gas flow rate was varied at a fixed catalyst mass (0.5 g). To investigate the influence of carbon dioxide on catalytic performance, we replaced part of the N_2 in the reactant feed with CO_2, giving a $C_2H_6/O_2/N_2/CO_2$ molar ratio = 2/1/3.7/1.7 (CO_2 composition = ca. 20 mol%) and a space velocity = 6000 mL h^{-1} g^{-1}. Ethane conversion and ethene, methane, carbon monoxide, and carbon dioxide selectivities were calculated based on the balance of carbon (23). The balances of carbon and oxygen were estimated to be 100 ± 2 and 100 ± 3%, respectively, for every run over the catalysts.

The crystal phases of the catalysts were determined by X-ray powder diffraction (XRD, D-MAX, Rigaku Rotaflex) operating at 40 kV and 40 mA using Cu$K\alpha$ radiation filtered with a nickel monochromator. X-ray photoelectron spectroscopy (XPS, Leybold Heraeus-Shengyang SKL-12) was used to characterize the catalyst surfaces. The surface contents of halides in the catalysts were calculated according to the approach described in Ref. (24). The specific surface areas of the catalysts were measured (using a NOVA 1200 apparatus) and calculated according to the BET method. The continuous flow chromatographic technique was adopted with helium as the carrier gas and nitrogen as the adsorbate. The halogen contents were analyzed according to the procedures reported in Ref. (24).

For the TPD of oxygen and carbon dioxide, the sample (0.2 g) was placed in the middle of a quartz microreactor (i.d. = 4 mm). The outlet gases were analyzed on line by mass spectrometry (HP G1800A). The heating rate was 10°C min^{-1} and the temperature range was from room temperature to 850°C. Before performing an O_2-TPD experiment, the sample was first calcined *in situ* at 850°C for 30 min in an oxygen flow of 15 mL min^{-1}, followed by cooling in oxygen to room temperature and then purging with helium (flow rate, 20 mL min^{-1}) for 30 min. Before a CO_2-TPD experiment, the catalyst was first calcined *in situ* at 850°C for 20 min under an oxygen flow of 15 mL min^{-1}, followed by purging with helium (20 mL min^{-1}) for 30 min and cooling in helium to room temperature before exposure to a flow of CO_2 gas (20 mL min^{-1}) for 10 min at room temperature and helium purging afterward for 20 min. The quantification of O_2 or CO_2 desorbed from the catalysts was made by calibrating the peak areas against a standard pulse of O_2 or CO_2.

TPR was conducted by using a 7% H_2–93% N_2 (v/v) gas mixture. The flow rate of the carrier gas was 50 mL min^{-1} and a thermal conductivity detector was employed. The amount of the sample used was 0.2 g and the heating rate was 10°C min^{-1}. Before performing the TPR experiments, the sample was first calcined *in situ* at 850°C for 30 min in an oxygen flow of 15 mL min^{-1} followed by cooling in oxygen to room temperature.

In situ laser Raman experiments were performed using a Nicolet 560 FT Laser Raman spectrometer. The samples were treated in O_2, N_2, H_2, C_2H_6, or $C_2H_6/O_2/N_2$ (molar ratio, 2/1/3.7) at different temperatures. After various treatments, the samples were monitored at 25°C without being exposed to air. The EPR experiments were carried out on a JES-TE100 spectrometer. Samples (ca. 1.5 g) treated under various conditions were examined in the X band at 25°C. The EPR system was equipped with a quartz-tube reactor that was transferable conveniently between the sample chamber and an oven. The sample in the quartz reactor could be heated to 800°C and exposed to gas(es) without being exposed to air.

RESULTS

Catalytic Performances of MO- and BaX_2-Promoted Y_2O_3 Catalysts

Tables 1 and 2 show the catalytic performances of MO, Y_2O_3, 30 mol% MO/Y_2O_3 (M = Mg, Ca, Sr, and Ba), and 30 mol% BaX_2/Y_2O_3 (X = F, Cl, and Br) catalysts for the ODE reaction. From Table 1, one can realize that quartz sands, BaO, BaF_2, $BaCl_2$, and $BaBr_2$ showed low C_2H_6 conversions (<6%) and high C_2H_4 selectivities (80–92%) at 640°C. The undoped Y_2O_3 gave 62.2% C_2H_6 conversion and 59.0% C_2H_4 selectivity, showing a C_2H_4 yield of 36.7%. With the addition of 30 mol% of MO to Y_2O_3, C_2H_6 conversions decreased (except for BaO, a 30 mol% BaO/Y_2O_3 catalyst showed 62.9% C_2H_6 conversion, 68.1% C_2H_4 selectivity, and 42.8% C_2H_4 yield) and C_2H_4 selectivities increased significantly. The addition of 30 mol% of $BaCO_3$ to Y_2O_3 caused both the C_2H_6 conversion and C_2H_4 selectivity to decrease. Based on the fact that BaO was the most effective in promoting Y_2O_3, we used BaX_2 (X = F, Cl, and Br) as dopants to modify Y_2O_3. Over the 30 mol% BaF_2/Y_2O_3 and 30 mol% $BaBr_2/Y_2O_3$ catalysts, C_2H_6 conversions were 50.0 and 57.1%, respectively, while C_2H_4 selectivities were 73.5 and 77.7%. As for the 30 mol% $BaCl_2/Y_2O_3$ catalyst, C_2H_6 conversion was 72.1% and C_2H_4 selectivity was 73.6%. The O_2 conversions over the Y_2O_3, MO/Y_2O_3, $BaCO_3/Y_2O_3$, and BaF_2/Y_2O_3 catalysts were close to 100%, whereas over the 30 mol% $BaCl_2/Y_2O_3$ and 30 mol% $BaBr_2/Y_2O_3$ catalysts they were 88.2 and 87.6%, respectively.

From Table 2, one can observe that the C_2H_6 conversion over pure Y_2O_3 was higher than those over the modified catalysts at temperatures below 600°C. With the rise in temperature from 600 to 640°C, C_2H_6 conversion, and C_2H_4 selectivity over Y_2O_3, 30 mol% BaO/Y_2O_3, and 30 mol% BaX_2/Y_2O_3 increased. For the pure Y_2O_3, 30 mol% BaO/Y_2O_3, 30 mol% BaF_2/Y_2O_3, and 30 mol% $BaBr_2/Y_2O_3$ catalysts, O_2 conversions increased with the increase in temperature, whereas for 30 mol% $BaCl_2/Y_2O_3$ O_2 conversion first decreased and then increased. The C_2H_4 yields of the 30 mol% BaO/Y_2O_3, 30 mol% $BaCl_2/Y_2O_3$, and 30 mol% $BaBr_2/Y_2O_3$ catalysts were 42.8, 53.1, and 44.4% at 640°C, respectively.

Table 3 shows the results of the oxidation of C_2H_4 and C_2H_6, respectively, over the Y_2O_3, 30 mol% BaO/Y_2O_3, and BaX_2/Y_2O_3 catalysts at 640°C. With the addition of BaO or BaX_2 to Y_2O_3, C_2H_4 selectivity increased in the ODE reaction, whereas C_2H_4 conversion decreased in the oxidation of ethene, especially over the three halide-promoted catalysts. In other words, the presence of halide ions can retard the process of ethene deep oxidation.

The catalytic activities of 30 mol% BaX_2/Y_2O_3 calcined, respectively, at 800, 900, and 1000°C are shown in Table 4. With the increase of calcination temperature, C_2H_4 selectivities increased and O_2 conversions decreased over the three catalysts; C_2H_6 conversion increased for the BaF_2-doped catalyst but decreased for the $BaBr_2$-doped catalyst whereas there was a maximum value of 72.1% for the $BaCl_2$-promoted Y_2O_3 catalyst. The $BaCl_2$- and $BaBr_2$-modified catalysts calcined at 900°C showed a maximum C_2H_4 yield of 53.1 and 44.4%, respectively. The performance of the 30 mol% BaF_2/Y_2O_3 catalyst calcined at 900°C was slightly inferior to that calcined at 1000°C.

Table 5 shows the catalytic performances of 30 mol% BaO/Y_2O_3 and 30 mol% BaX_2/Y_2O_3 with respect to

TABLE 1

The Catalytic Performances after an On-Stream Time of 1 h over Y_2O_3, 30 mol% MO/Y_2O_3 (M = Mg, Ca, Sr, and Ba), 30 mol% BaX_2/Y_2O_3 (X = F, Cl, and Br), and 30 mol% $BaCO_3/Y_2O_3$ at 640°C

Catalyst	Conversion (%)		Selectivity (%)			Yield (%)	Rate of C_2H_6 reaction
	C_2H_6	O_2	CO_x[a]	CH_4	C_2H_4	C_2H_4	(10^{18} molecules m^{-2} s^{-1})
Blank[b]	5.0	—	12.0	0	88.0	4.4	—
Y_2O_3	62.2	99.8	36.7	4.3	59.0	36.7	0.118
MgO/Y_2O_3	44.3	98.1	30.3	3.6	66.1	29.3	0.149
CaO/Y_2O_3	53.4	96.4	25.8	5.4	68.8	36.7	0.174
SrO/Y_2O_3	51.4	94.1	24.0	5.2	70.8	36.4	0.168
BaO/Y_2O_3	62.9	95.9	27.3	4.6	68.1	42.8	0.208
$BaCO_3/Y_2O_3$	41.9	99.0	41.4	4.7	53.9	22.6	0.145
BaO	19.3	72.1	14.0	3.0	82.9	16.0	—
BaF_2	5.5	20.4	6.2	1.6	92.2	5.1	—
$BaCl_2$	1.9	12.6	20.0	0.0	80.0	1.5	—
$BaBr_2$	1.4	12.4	14.3	0.0	85.7	1.2	—
BaF_2/Y_2O_3	50.0	96.8	24.0	2.5	73.5	36.7	0.326
$BaCl_2/Y_2O_3$	72.1	88.2	23.5	2.9	73.6	53.1	0.281
$BaBr_2/Y_2O_3$	57.1	87.6	19.0	3.3	77.7	44.4	0.191

[a] $CO_x = CO + CO_2$.
[b] tested at 660°C.

TABLE 2

Catalytic Performances of Undoped Y_2O_3, 30 mol% BaO/Y_2O_3, and 30 mol% BaX_2/Y_2O_3 (X = F, Cl, and Br) Catalysts at Temperatures Ranging from 560 to 660°C

Catalyst	Temp. (°C)	Conversion (%)		Selectivity (%)			Yield (%), C_2H_4	Rate of C_2H_6 reaction (10^{18} molecules m^{-2} s^{-1})
		C_2H_6	O_2	CO_x	CH_4	C_2H_4		
Y_2O_3	560	46.0	99.0	49.1	2.4	48.5	22.3	0.087
	600	54.8	100	42.5	3.0	54.5	29.9	0.104
	620	56.8	100	38.1	3.5	58.4	33.1	0.107
	640	62.2	100	36.7	4.3	59.0	36.7	0.118
	660	66.5	100	36.0	5.6	58.3	38.8	0.126
BaO/Y_2O_3	560	16.8	61.8	37.3	1.4	63.6	10.7	0.056
	600	44.3	89.8	29.5	2.6	68.0	30.1	0.147
	620	52.7	94.2	27.9	3.3	68.9	36.3	0.174
	640	62.9	95.9	27.3	4.6	68.1	42.8	0.208
	660	63.5	96.8	26.3	6.5	67.2	42.7	0.210
BaF_2/Y_2O_3	560	23.5	79.5	42.2	1.8	56.0	13.2	0.153
	600	45.3	94.8	29.7	2.6	67.7	30.7	0.296
	620	48.9	95.7	26.5	2.9	70.6	34.5	0.319
	640	50.0	96.8	24.0	2.5	73.5	36.7	0.326
	660	51.8	100	21.9	3.7	74.4	38.5	0.338
$BaCl_2/Y_2O_3$	560	44.1	97.8	43.6	2.6	53.8	23.7	0.172
	600	52.3	94.3	36.4	2.8	61.8	32.3	0.204
	620	61.1	91.6	29.4	3.0	67.6	41.3	0.220
	640	72.1	88.2	23.5	2.9	73.6	53.1	0.281
	660	67.1	92.1	26.7	3.2	70.1	47.0	0.261
$BaBr_2/Y_2O_3$	560	44.7	83.2	26.9	2.4	70.7	31.6	0.150
	600	52.7	86.9	21.1	2.8	76.0	40.1	0.177
	620	55.3	87.2	18.7	2.9	78.4	43.3	0.185
	640	57.1	87.6	19.0	3.3	77.7	44.4	0.191
	660	60.7	89.9	20.6	3.6	75.8	45.9	0.203

on-stream reaction time under the conditions $C_2H_6/O_2/N_2/CO_2$ molar ratio = 2/1/3.7/1.7 (corresponding to a CO_2 content of ca. 20 mol%), temperature = 640°C, and space velocity = 6000 mL h^{-1} g^{-1}. With the prolongation of reaction time, the BaO-modified Y_2O_3 catalyst degraded more rapidly than the BaF_2- and $BaBr_2$-modified Y_2O_3 catalysts. After 40 h of on-stream reaction, the latter two catalysts showed activities rather close to that of a 30 mol% $BaCO_3/Y_2O_3$ catalyst (Table 1); the 30 mol% $BaCl_2/Y_2O_3$ catalyst, however, underwent only a slight decrease in catalytic performance.

Figure 1 shows the catalytic performances of BaO/Y_2O_3, $BaCl_2/Y_2O_3$, and $BaBr_2/Y_2O_3$ as related to the respective loading of BaO, $BaCl_2$, and $BaBr_2$. Over the three catalysts, with the increase in BaO, $BaCl_2$, or $BaBr_2$ loading, C_2H_4 selectivity increased whereas O_2 conversion and CO_x selectivity decreased. With increasing BaO or $BaCl_2$ loading, C_2H_6 conversion and C_2H_4 yield first increased and then decreased, reaching maximum values (respectively, 62.9 and 42.8% for BaO/Y_2O_3; 72.1 and 53.1% for $BaCl_2/Y_2O_3$) at 30 mol% (Figs. 1a and 1b). From Fig. 1c, one can observe that over the $BaBr_2/Y_2O_3$ catalyst, C_2H_6 conversion decreased monotonously with the increase in $BaBr_2$ loading; C_2H_4 yield, on the other hand, first increased and then decreased, with a maximum value of 44.4% being observed at 30 mol% of $BaBr_2$ loading.

Figure 2 shows the catalytic performances of 30 mol% BaO/Y_2O_3, 30 mol% $BaCl_2/Y_2O_3$, and 30 mol% $BaBr_2/Y_2O_3$ during 40 h of on-stream ODE reactions at 640°C. As shown in Figs. 2a and 2c, over the 30 mol% BaO/Y_2O_3 and

TABLE 3

The Catalytic Performances of Y_2O_3, 30 mol% BaO/Y_2O_3, 30 mol% BaX_2 (X = F, Cl, and Br)/Y_2O_3 Catalysts in Ethane and Ethene Oxidations at 640°C

Catalyst	Oxidation of C_2H_4[a]	Oxidation of C_2H_6	
	C_2H_4 Conv. (%)	C_2H_6 Conv. (%)	C_2H_4 Sel. (%)
Y_2O_3	30.8	62.2	59.0
BaO/Y_2O_3	25.1	62.9	68.1
BaF_2/Y_2O_3	18.2	50.0	73.5
$BaCl_2/Y_2O_3$	17.9	72.1	73.6
$BaBr_2/Y_2O_3$	15.6	57.1	77.7

[a] At $C_2H_4/O_2/N_2$ = 2/1/3.7 and space velocity = 6000 mL h^{-1} g^{-1}.

TABLE 4

The Properties and Catalytic Performances of 30 mol% BaX_2/Y_2O_3 Calcined (6 h) at 800, 900, and 1000°C

Catalyst:	BaF_2/Y_2O_3			$BaCl_2/Y_2O_3$			$BaBr_2/Y_2O_3$		
Calcination temperature (°C):	800	900	1000	800	900	1000	800	900	1000
C_2H_6 Conversion (%)	48.2	50.0	51.4	63.6	72.1	50.4	58.8	57.1	54.6
O_2 Conversion (%)	100	100	99.8	90.8	88.2	65.4	94.8	87.6	86.2
C_2H_4 Selectivity (%)	68.8	73.5	74.0	60.6	73.6	75.7	73.7	77.7	78.1
CH_4 Selectivity (%)	2.8	3.5	3.7	2.4	2.9	2.5	2.8	3.3	3.6
CO_x Selectivity (%)	28.4	23.0	22.3	37.0	23.5	23.8	23.5	19.0	18.3
C_2H_4 Yield (%)	33.2	36.8	38.0	38.5	53.1	38.1	43.3	44.4	42.6
Y_2O_3 Lattice parameter, a_0 (Å)	10.608	10.611	10.613	10.618	10.631	10.610	10.614	10.624	10.613
BaX_2 Lattice parameter, a (Å)	6.188	6.187	6.185	6.704	6.684	6.698	10.430	10.419	10.432
b (Å)	—	—	—	10.899	10.882	10.891	7.196	7.173	7.199
c (Å)	—	—	—	7.128	7.112	7.124	8.373	8.360	8.374
Surface X composition (wt%)	26.26	26.18	25.98	9.15	8.91	7.99	18.52	18.32	14.36
Bulk X composition (wt%)	5.21	5.10	4.88	9.10	8.85	7.91	19.12	18.44	15.18
Surface area ($m^2\ g^{-1}$)	3.36	3.04	2.80	5.21	5.10	4.32	6.23	5.92	4.24

30 mol% $BaBr_2/Y_2O_3$ catalysts, C_2H_6 conversions, C_2H_4 selectivities, and C_2H_4 yields decreased, whereas O_2 conversions increased with reaction time. After 40 h, C_2H_6 conversion, C_2H_4 selectivity, and C_2H_4 yield dropped from 62.9, 68.1, and 42.8%, respectively, to 47.7, 53.2, and 25.4% over 30 mol% BaO/Y_2O_3. The respective drops were ca. 18, 12, and 28% over the 30 mol% $BaBr_2/Y_2O_3$ catalyst. The degraded performances of the two catalysts were only slightly better than that of a 30 mol% $BaCO_3/Y_2O_3$ sample. The catalytic performance of a 30 mol% $BaCl_2/Y_2O_3$ (Fig. 2b), however, was stable within a period of 40 h.

Figure 3 shows the influence of space velocity on the catalytic performance of 30 mol% $BaCl_2/Y_2O_3$ at 640°C. With the change in contact time (1/SV) from 2.5×10^{-4} to 1.0×10^{-4} h g mL^{-1}, C_2H_6 conversion decreased from 76.6 to 64.7% and O_2 conversion decreased from 92.9 to 79.1%; the C_2H_4 selectivity increased from 64.2 to 80.1%. The highest C_2H_4 yield of 53.7% was achieved at 1.25×10^{-4} h g mL^{-1}. When the catalyst was dispersed in quartz sand (40–80 mesh, 5.0 g), we observed similar results.

BET, XRD, and XPS Studies

The properties of the 30 mol% BaX_2/Y_2O_3 catalysts calcined, respectively, at 800, 900, and 1000°C are also shown in Table 4. The crystal structure of Y_2O_3 is of fluorite type (25), the length (a_0) of the unit cell edge is 10.604 Å. BaF_2 is cubic, the lattice parameter (a_0) is 6.200 Å. Crystals of $BaCl_2 \cdot 2H_2O$ and $BaBr_2 \cdot 2H_2O$ are monoclinic; the lattice parameters (a, b, and c) are 6.720, 10.907, and 7.135 Å and 10.442, 7.207, and 8.384 Å, respectively. From Table 4, one can observe that the 30 mol% $BaCl_2/Y_2O_3$ and 30 mol% $BaBr_2/Y_2O_3$ catalysts calcined at 900°C and the 30 mol% BaF_2/Y_2O_3 catalyst calcined at 1000°C showed the largest lattice parameter a_0 of cubic Y_2O_3, respectively. As for the contraction of barium halide lattice, it was the most significant in the $BaCl_2$- and $BaBr_2$-modified Y_2O_3 catalysts calcined at 900°C and in the BaF_2-doped Y_2O_3 catalyst calcined at 1000°C. With the increase in calcination temperature from 800 to 1000°C, the surface and bulk halide compositions as well as the

TABLE 5

The Catalytic Performances of 30 mol% BaO/Y_2O_3 and 30 mol% BaX_2/Y_2O_3 with Respect to On-Stream Reaction Time

	1 h			10 h			20 h			40 h		
Catalyst	C_2H_6 Conv. (%)	C_2H_4 Sel. (%)	C_2H_4 Yield (%)	C_2H_6 Conv. (%)	C_2H_4 Sel. (%)	C_2H_4 Yield (%)	C_2H_6 Conv. (%)	C_2H_4 Sel. (%)	C_2H_4 Yield (%)	C_2H_6 Conv. (%)	C_2H_4 Sel. (%)	C_2H_4 Yield (%)
BaO/Y_2O_3	59.2	61.1	36.2	52.4	56.0	29.3	44.6	54.2	24.2	42.5	52.9	22.5
BaF_2/Y_2O_3	49.5	72.9	36.1	48.2	70.3	33.9	46.0	67.1	30.9	44.4	60.2	26.7
$BaCl_2/Y_2O_3$	71.9	72.8	52.3	71.5	72.6	51.9	71.2	71.9	51.2	70.7	71.2	50.3
$BaBr_2/Y_2O_3$	56.8	76.7	43.6	55.4	73.8	40.9	51.1	69.6	35.5	46.2	64.6	29.8

Note. At $C_2H_6/O_2/N_2/CO_2$ molar ratio = 2/1/3.7/1.7, temperature = 640°C, and space velocity = 6000 mL $h^{-1}\ g^{-1}$.

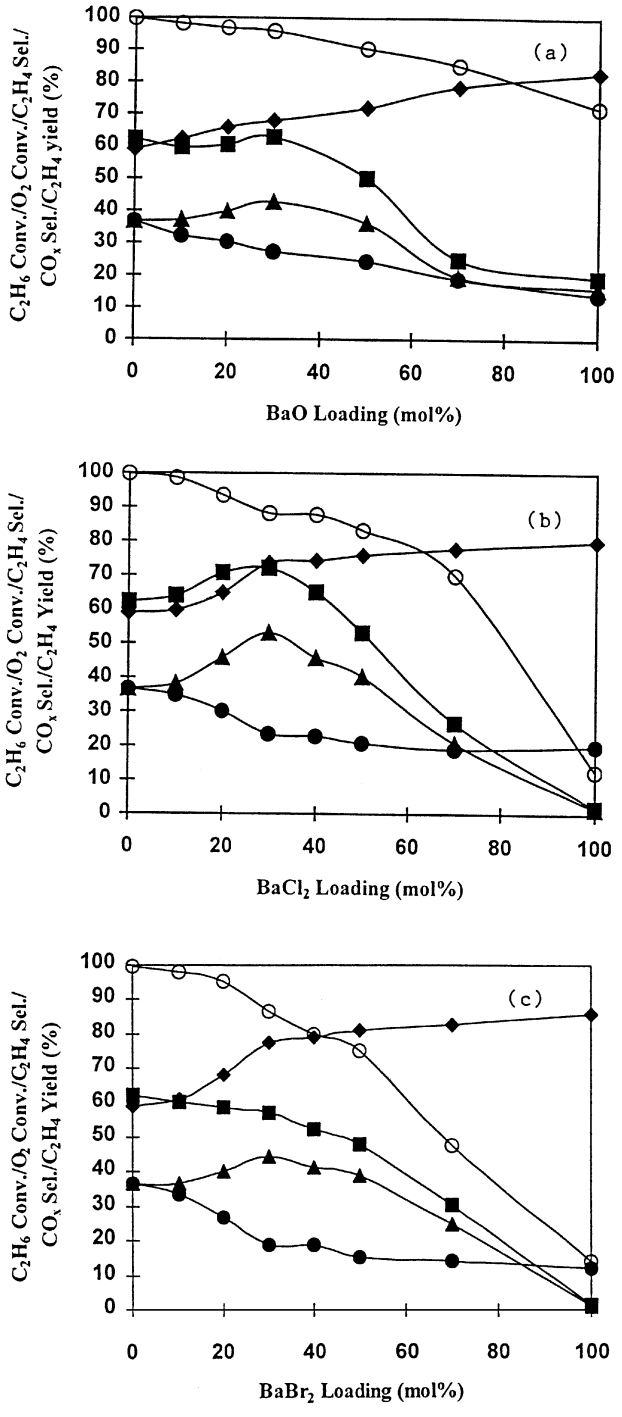

FIG. 1. The catalytic performances of (a) 30 mol% BaO/Y_2O_3, (b) 30 mol% $BaCl_2/Y_2O_3$, and (c) 30 mol% $BaBr_2/Y_2O_3$ catalysts as related to BaO or BaX_2 loading at 640°C. (■) C_2H_6 conversion, (◆) C_2H_4 selectivity, (▲) C_2H_4 yield, (●) CO_x selectivity, (○) O_2 conversion.

specific surface area decreased. For the BaF_2-doped catalyst, the surface F^- content was much higher than the bulk F^- content; for the $BaBr_2$-doped catalyst, the surface Br^- composition was lower than the bulk Br^- composition; for the $BaCl_2$-modified catalysts, however, the bulk and surface Cl concentrations were rather similar. In other words, Cl^- ions were uniformly distributed throughout the 30 mol% $BaCl_2/Y_2O_3$ catalysts.

Table 6 shows the surface areas and crystal phases of the fresh and used (ODE reaction at 640°C for 8 or 40 h) Y_2O_3, and 30 mol% BaO/Y_2O_3, and 30 mol% BaX_2/Y_2O_3 catalysts. After the ODE reactions, the surface areas of the respective catalysts decreased by ca. 33, 38, 46, 3, and 33%. No new phases such as barium and yttrium haloxides were

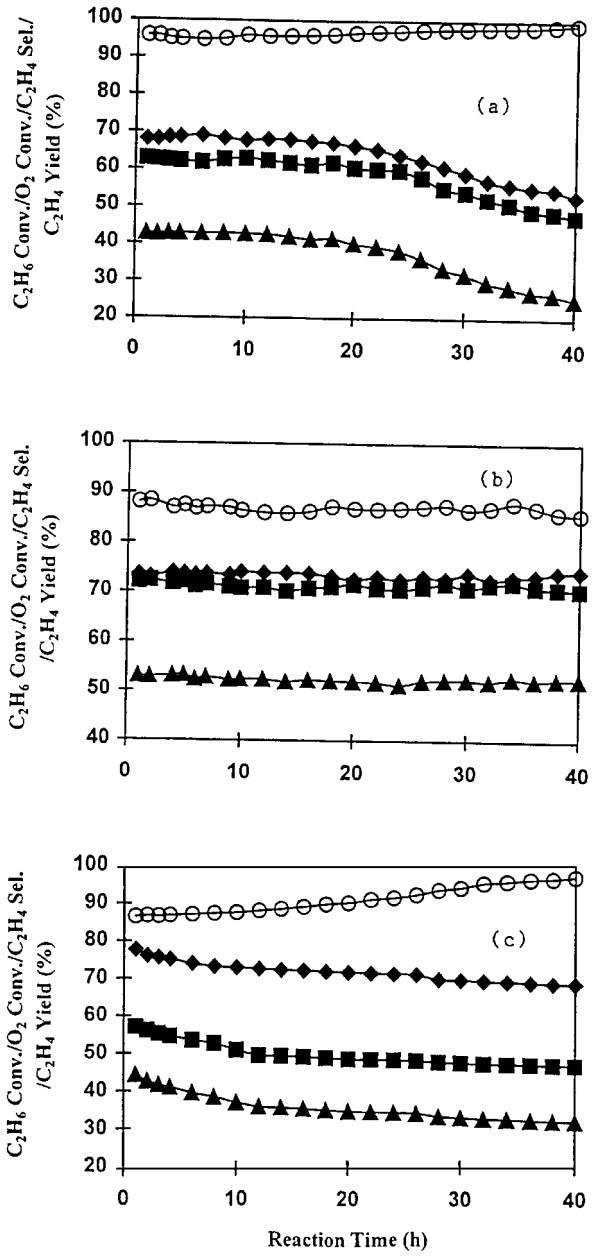

FIG. 2. Lifetime study of (a) 30 mol% BaO/Y_2O_3, (b) 30 mol% $BaCl_2/Y_2O_3$, and (c) 30 mol% $BaBr_2/Y_2O_3$ catalysts during 40 h of on-stream ODE reaction at 640°C. (■) C_2H_6 conversion, (◆) C_2H_4 selectivity, (▲) C_2H_4 yield, (○) O_2 conversion.

TABLE 6

Crystal Phases and Surface Areas of Y_2O_3, 30 mol% BaO/Y_2O_3, 30 mol% BaF_2/Y_2O_3, 30 mol% $BaCl_2/Y_2O_3$ and 30 mol% $BaBr_2/Y_2O_3$ Catalysts Observed before and after ODE Reaction at 640°C for 40 h

Catalyst	Crystal phase[a]		Surface area ($m^2\ g^{-1}$)	
	Before	After	Before	After
Y_2O_3[b]	Y_2O_3 (s)	Y_2O_3 (s)	10.50	7.04
BaO/Y_2O_3	Y_2O_3 (s), BaO (m), $BaCO_3$ (w)	Y_2O_3 (s), $BaCO_3$ (m)	6.00	3.74
BaF_2/Y_2O_3	Y_2O_3 (s), BaF_2 (m)	Y_2O_3 (s), $BaCO_3$ (w), BaF_2 (m)	3.04	1.63
$BaCl_2/Y_2O_3$	Y_2O_3 (s), $BaCl_2 \cdot 2H_2O$ (m)	Y_2O_3 (s), $BaCO_3$ (vw), $BaCl_2 \cdot 2H_2O$ (m)	5.10	4.94
$BaBr_2/Y_2O_3$	Y_2O_3 (s), $BaBr_2 \cdot 2H_2O$ (m)	Y_2O_3 (s), $BaCO_3$ (m), $BaBr_2 \cdot 2H_2O$ (m)	5.92	3.94

[a] Y_2O_3 is cubic. BaO is tetragonal. $BaCO_3$ is orthorhombic. BaF_2 is cubic. $BaCl_2 \cdot 2H_2O$ and $BaBr_2 \cdot 2H_2O$ are monoclinic. s, strong; m, medium; w, weak; vw, very weak.
[b] Reaction lasted 8 h.

detected by XRD in the 30 mol% BaX_2-promoted catalysts. After 40 h of ODE reaction, weak signals of orthorhombic $BaCO_3$ were detected over 30 mol% BaF_2/Y_2O_3. The tetragonal BaO phase in 30 mol% BaO/Y_2O_3 disappeared, whereas the originally weak signals of the $BaCO_3$ phase intensified. $BaCO_3$ signals of medium intensity were detected over 30 mol% $BaBr_2/Y_2O_3$. However, only very weak signals of $BaCO_3$ phase could be detected over the 30 mol% $BaCl_2/Y_2O_3$ catalyst.

Table 7 shows the surface and bulk halide compositions of the 30 mol% BaX_2/Y_2O_3 (X = F, Cl, and Br) catalysts. After 40 h of on-stream ODE reaction, the surface concentrations of F in 30 mol% BaF_2/Y_2O_3 and Cl in 30 mol% $BaCl_2/Y_2O_3$ decreased by 22.3 and 0.2%, respectively, of the original values, whereas the Br surface concentration of 30 mol% $BaBr_2/Y_2O_3$ increased by 3.2%. As for the F, Cl, and Br bulk concentrations, they decreased, respectively, by 4.5, 0.7, and 52.1%.

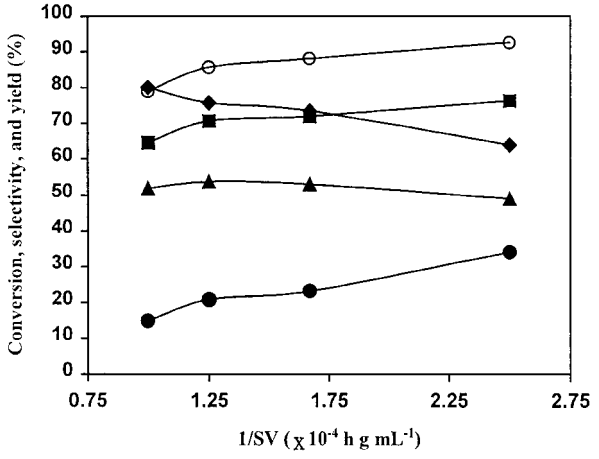

FIG. 3. The catalytic performance of 30 mol% $BaCl_2/Y_2O_3$ catalyst as related to the reciprocal of space velocity (SV) at 640°C. (■) C_2H_6 conversion, (◆) C_2H_4 selectivity, (▲) C_2H_4 yield, (●) CO_x selectivity, and (○) O_2 conversion.

TPD and TPR Studies

Figure 4 shows the CO_2-TPD profiles of fresh Y_2O_3 and 30 mol% $BaCO_3/Y_2O_3$ samples as well as fresh and used (after 40 h of ODE reaction) 30 mol% BaO/Y_2O_3 and 30 mol% BaX_2/Y_2O_3 samples. For Y_2O_3, there were desorption peaks at ca. 84, 102, 175, and 324°C, the total amount of CO_2 desorbed was 259.4 μmol g^{-1}; when temperature exceeded 744°C, large CO_2 desorption took place (Fig. 4a). For a 30 mol% $BaCO_3/Y_2O_3$ sample, there were small desorption peaks at ca. 82, 122, and 187°C, the total amount of CO_2 desorbed was 203.8 μmol g^{-1}; at ca. 660°C, large CO_2 desorption began (Fig. 4b). For a fresh 30 mol% BaO/Y_2O_3 sample, a large peak at 87°C and a small one at 150°C appeared (amount to 241.6 μmol g^{-1} CO_2 desorption), and at 705°C, large desorption began. For a used 30 mol% BaO/Y_2O_3 sample, a large peak at ca. 91°C with two small shoulders at ca. 133 and 190°C appeared, the desorbed amount was 277.9 μmol g^{-1}, and at ca. 661°C, large desorption took place (Figs. 4c and 4c′). For 30 mol% BaF_2/Y_2O_3,

TABLE 7

The Surface and Bulk Halide Compositions of 30 mol% BaX_2/Y_2O_3 Catalysts

Catalyst	Surface X composition (wt%)		Bulk X composition (wt%)	
	Before	After[a]	Before	After[a]
BaF_2/Y_2O_3	26.18	20.33	5.10	4.87
$BaCl_2/Y_2O_3$	8.91	8.89	8.85	8.79
$BaBr_2/Y_2O_3$	18.32	18.91	18.44	8.83

[a] After 40 h of ODE reaction at 640°C.

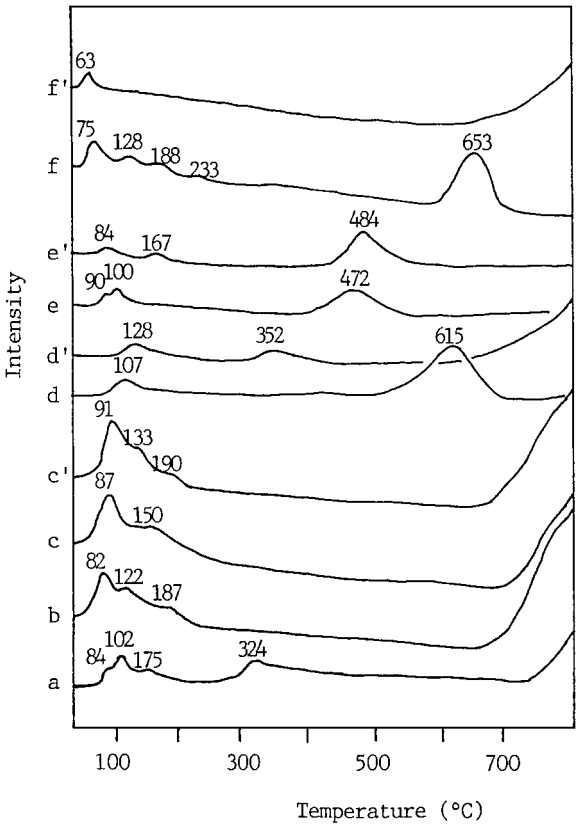

FIG. 4. CO_2-TPD profiles of fresh (a–f) and used (c′–f′) (after 40 h of ODE reaction) samples. (a) Y_2O_3, (b) 30 mol% $BaCO_3/Y_2O_3$, (c, c′) 30 mol% BaO/Y_2O_3, (d, d′) 30 mol% BaF_2/Y_2O_3, (e, e′) 30 mol% $BaCl_2/Y_2O_3$, and (f, f′) 30 mol% $BaBr_2/Y_2O_3$ samples.

the fresh sample showed a small desorption peak (37.1 μmol g^{-1}) at ca. 107°C and a large desorption peak (295.5 μmol g^{-1}) at ca. 615°C, whereas the used sample showed two small desorption peaks at ca. 128°C (39.1 μmol g^{-1}) and 352°C (26.6 μmol g^{-1}) and large CO_2 desorption began at ca. 630°C (Figs. 4d and 4d′). For a fresh 30 mol% $BaCl_2/Y_2O_3$ sample, there were two small desorption peaks (amount to 27.0 μmol g^{-1}) at ca. 90 and 100°C and a large one (118.1 μmol g^{-1}) at ca. 472°C, whereas the used catalyst showed two smaller peaks (amount to 24.6 μmol g^{-1}) at ca. 84 and 167°C and a large one (129.9 μmol g^{-1}) at ca. 484°C (Figs. 4e and 4e′). As for a fresh 30 mol% $BaBr_2/Y_2O_3$ sample, there were peaks at ca. 75, 128, 188, and 233°C (the total amount of desorbed CO_2 was 128.8 μmol g^{-1}) and a large one (210.2 μmol g^{-1}) at 653°C; a used one showed a small desorption peak (11.6 μmol g^{-1}) at ca. 63°C and large desorption started at ca. 640°C (Figs. 4f and 4f′).

Figure 5 shows the O_2-TPD profiles of fresh Y_2O_3, 30 mol% $BaCO_3/Y_2O_3$, 30 mol% BaO/Y_2O_3, 30 mol% BaX_2/Y_2O_3 (X = F and Br), and fresh and used (40 h of ODE reaction) 30 mol% $BaCl_2/Y_2O_3$ samples. For each of the fresh Y_2O_3 and 30 mol% BaX_2/Y_2O_3 (X = F, Cl, and Br) samples, there was only one O_2 desorption peak centered, respectively, at ca. 432, 530, 463, and 455°C; the corresponding amounts were 1.33, 2.37, 2.88, and 2.43 μmol g^{-1}. There were two desorptions over the fresh 30 mol% $BaCO_3/Y_2O_3$ (at ca. 442 and 517°C, totally 9.64 μmol g^{-1}) and 30 mol% BaO/Y_2O_3 (at ca. 473 and 566°C, totally 17.66 μmol g^{-1}) samples (Figs. 5e and 5f). After 40 h of on-stream ODE reaction, the O_2 desorption peak recorded over the fresh 30 mol% BaX_2/Y_2O_3 (X = F and Br) samples decreased in intensity and shifted to higher temperatures (not shown). The used 30 mol% $BaCl_2/Y_2O_3$ catalyst exhibited an O_2 desorption peak (2.83 μmol g^{-1}) at ca. 454°C with intensity similar to that obtained over the fresh one (Fig. 5d′).

Figure 6 shows the TPR profiles of Y_2O_3, 30 mol% BaO/Y_2O_3, and 30 mol% BaX_2/Y_2O_3. For Y_2O_3, a broad TPR band of relatively weak intensity stretching from 300 to 600°C was observed. For 30 mol% BaO/Y_2O_3, there was a large reduction peak at ca. 485°C and a weak one at ca. 680°C, and there was still reduction above 750°C (Fig. 6b). For the 30 mol% BaF_2/Y_2O_3 catalyst, reduction started at ca. 320°C and continued well above 800°C (Fig. 6c). A reduction peak of moderate intensity could be observed at ca. 480°C over 30 mol% $BaCl_2/Y_2O_3$. For 30 mol% $BaBr_2/Y_2O_3$, a weak reduction peak stretching from 430 to 780°C was observed (Fig. 6e). It is difficult to quantify the TPR bands.

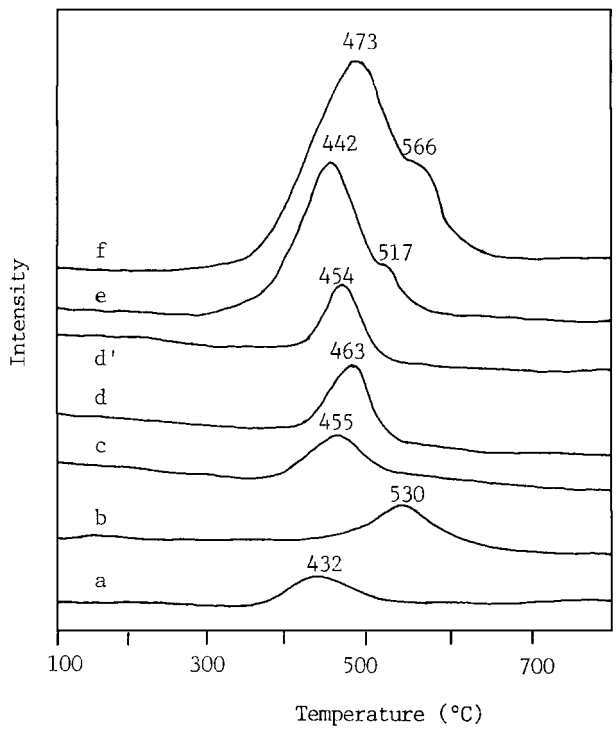

FIG. 5. O_2-TPD profiles of (a) fresh Y_2O_3, (b) fresh 30 mol% BaF_2/Y_2O_3, (c) fresh 30 mol% $BaBr_2/Y_2O_3$, (d) fresh and (d′) used (40 h of ODE reaction) 30 mol% $BaCl_2/Y_2O_3$, (e) fresh 30 mol% $BaCO_3/Y_2O_3$, and (f) fresh 30 mol% BaO/Y_2O_3 samples.

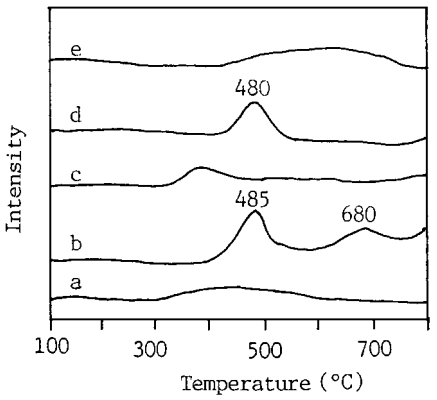

FIG. 6. TPR profiles of (a) Y_2O_3, (b) 30 mol% BaO/Y_2O_3, (c) 30 mol% BaF_2/Y_2O_3, (d) 30 mol% $BaCl_2/Y_2O_3$, and (e) 30 mol% $BaBr_2/Y_2O_3$ samples.

In Situ Laser Raman Studies

Figure 7 shows the laser Raman spectra of a 30 mol% BaO/Y_2O_3 sample recorded after various treatments. When the sample was treated in an O_2 flow at 800°C for 20 min, Raman bands were observed at ca. 694, 842, 1026, 1062, and 1387 cm^{-1} (Fig. 7a). The bands at ca. 694 and 1062 cm^{-1} could be assigned to CO_3^{2-} species (26), the band at ca. 842 cm^{-1} to O_2^{2-} species (26, 27), the band at ca. 1026 cm^{-1} to O_2^{n-} O_2 ($1 < n < 2$) and/or O_2^{2-} species (18, 26), and the band at ca. 1387 cm^{-1} to $O_2^{\delta-}$ ($0 < \delta < 1$) species (26). In a flow of N_2 and with increase in treatment temperatures from 500 to 800°C, the bands, with the one at 1062 cm^{-1} being the exception, shifted slightly to higher wavenumbers and decreased in intensity (Figs. 7b to 7d). Treating the sample in C_2H_6 at 640°C for 30 min caused little change (Fig. 7e). The two bands at ca. 694 and 1055 cm^{-1} (CO_3^{2-}) could still be observed after the sample was treated in C_2H_6 at 700°C for 30 min (Fig. 7f); after further treatment in C_2H_6 at 750°C for 30 min, there was no observable Raman signal (Fig. 7g). However, with the treatment in O_2 at 800°C for 30 min, the signals of carbonate and oxygen species reappeared (Fig. 7h).

The Raman spectra of 30 mol% BaF_2/Y_2O_3 and 30 mol% $BaBr_2/Y_2O_3$ samples recorded after various treatments are shown in Figs. 8 and 9. When the samples were treated

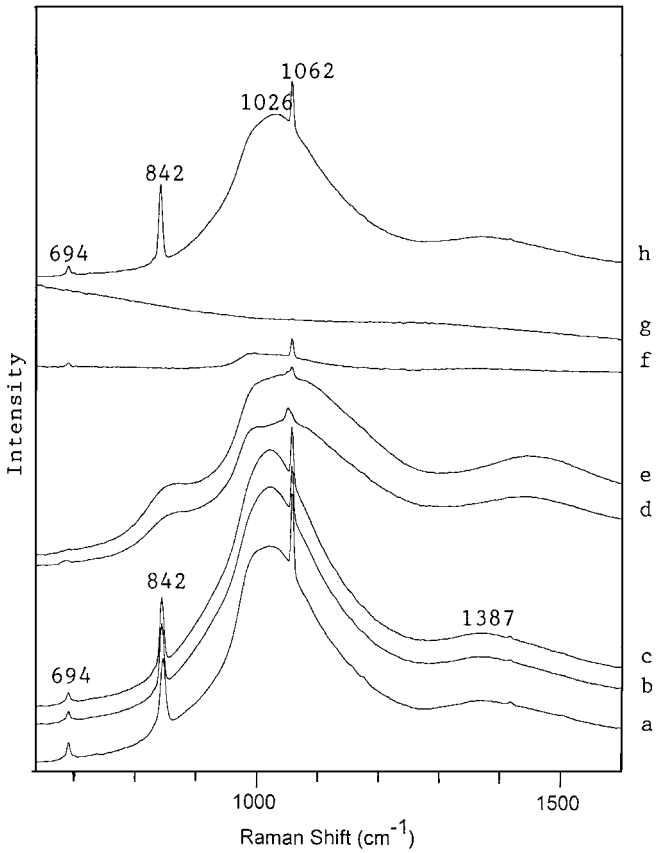

FIG. 7. Laser Raman spectra of a 30 mol% BaO/Y_2O_3 sample when it was treated: (a) in O_2 at 800°C for 20 min, (b) then in N_2 at 500°C for 20 min, (c) then in N_2 at 600°C for 20 min, (d) then in N_2 at 800°C for 20 min, (e) then in C_2H_6 at 640°C for 30 min, (f) then in C_2H_6 at 700°C for 30 min, (g) then in C_2H_6 at 750°C for 30 min, and (h) in O_2 at 800°C for 30 min.

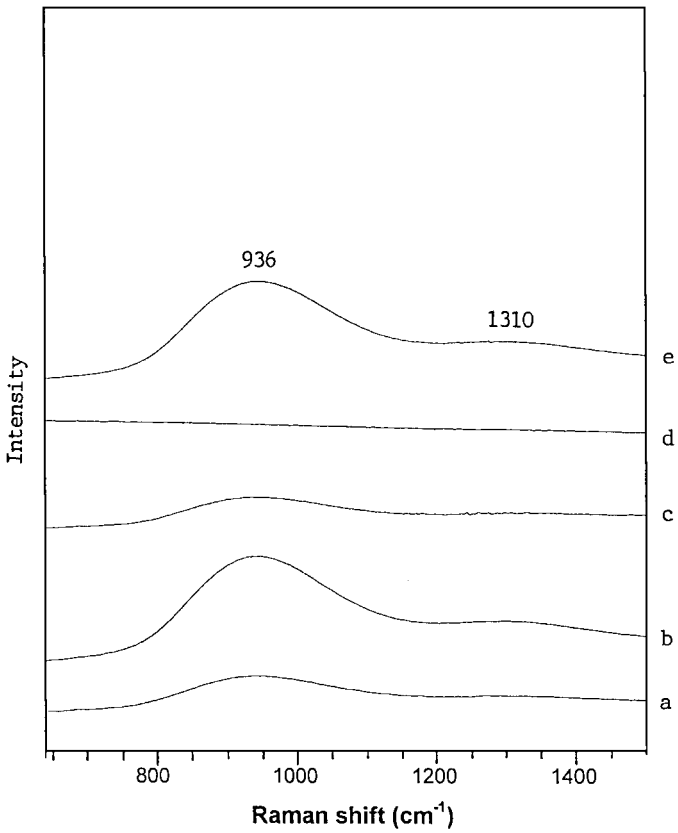

FIG. 8. Laser Raman spectra of a 30 mol% BaF_2/Y_2O_3 sample when it was treated: (a) in O_2 at 640°C for 30 min, (b) then in O_2 at 750°C for 30 min, (c) then in $C_2H_6/O_2/N_2$ (molar ratio, 2/1/3.7) at 640°C for 30 min, (d) then in C_2H_6 at 640°C for 30 min, and (e) then in O_2 at 750°C for 30 min.

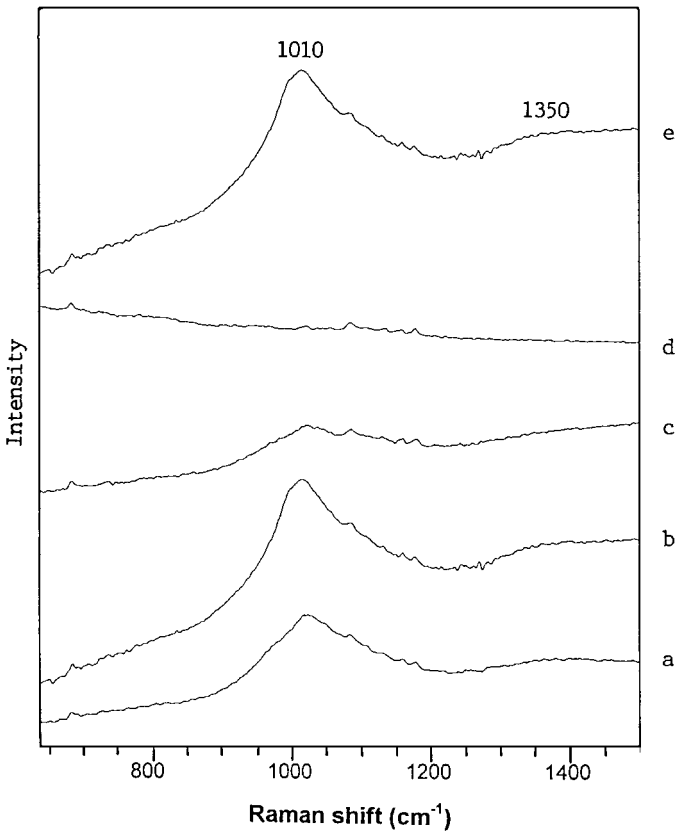

FIG. 9. Laser Raman spectra of a 30 mol% $BaBr_2/Y_2O_3$ sample when it was treated: (a) in O_2 at 640°C for 30 min, (b) then in O_2 at 750°C for 30 min, (c) then in $C_2H_6/O_2/N_2$ (molar ratio, 2/1/3.7) at 640°C for 30 min, (d) then in C_2H_6 at 640°C for 30 min, and (e) then in O_2 at 750°C for 30 min.

in O_2 at 640°C for 30 min, broad bands centered, respectively, at 936 cm^{-1} (Fig. 8a) and at ca. 1010 cm^{-1} (Fig. 9a) were observed; such Raman signals could be assigned to O_2^{n-} and/or O_2^{2-} (18). Further treatment in O_2 at 750°C for 30 min caused these two bands to increase in intensity and a weak signal could be observe at ca. 1310 cm^{-1} (Fig. 8b) and at ca. 1350 cm^{-1} (Fig. 9b), respectively, over the two catalysts; these signals could be ascribed to $O_2^{\delta-}$ (26). After a reactant mixture ($C_2H_6/O_2/N_2$ molar ratio = 2/1/3.7) was introduced to the samples at 640°C for 30 min, the bands at ca. 936 cm^{-1} (Fig. 8c) and ca. 1010 cm^{-1} (Fig. 9c) decreased in intensity, whereas the signals at ca. 1310 cm^{-1} (Fig. 9c) and ca. 1350 cm^{-1} (Fig. 9b) disappeared. Further treatment in C_2H_6 at 640°C for 30 min eliminated all the signals (Figs. 8d and 9d). With the treatment in O_2 at 750°C for 30 min, however, the signals of O_2^{n-} and/or O_2^{2-} and $O_2^{\delta-}$ species reappeared (Figs. 8e and 9e).

The spectrum of a 30 mol% $BaCl_2/Y_2O_3$ sample treated in N_2 at 600°C for 20 min was similar to that of a fresh sample in air at room temperature (Figs. 10a and 10b). When the sample was treated in O_2 for 30 min at temperatures ranging from 600 to 640°C, the band stretching from 900 to 1050 cm^{-1} increased in intensity (Figs. 10c and 10d). This band could be assigned to surface species such as O_2^{n-} and/or O_2^{2-} (18). The bands within the 1069–1178 cm^{-1} range could be assigned to the stretching vibration of O_2^- (28–32). When a reactant mixture ($C_2H_6/O_2/N_2 = 2/1/3.7$) was introduced to the sample at 640°C for 45 min (Fig. 10e), the band that stretched from 900 to 1050 cm^{-1} decreased in intensity and a small band appeared at ca. 740 cm^{-1} which might be ascribed to O_2^{2-} adspecies (27). When treated in O_2 at 750°C for 30 min, the band intensity at ca. 1000 cm^{-1} increased significantly (Fig. 10f). The bands at ca. 740 and 1000 cm^{-1} disappeared after the sample was treated in C_2H_6 at 640°C for 30 min (Fig. 10g). It should be noted that the band at ca. 686 cm^{-1} (sublayer O_2^{2-}) always appeared (Figs. 10a–10g). These results confirmed that surface dioxygen adspecies, O_2^{2-}, O_2^{n-}, O_2^-, and $O_2^{\delta-}$, were participating in the oxidation of C_2H_6.

EPR Studies

Figure 11 shows the EPR spectra of an undoped Y_2O_3 catalyst treated under various conditions. One can observe that due to variation in chemical environment, the g tensors of paramagnetic species (O^- and O_2^-) vary. The three spectra recorded when the sample was being treated progressively in air at room temperature for 1 h (Fig. 11a), in H_2 at 500°C for 1 h (Fig. 11b), and in H_2 at 700°C for 1 h (Fig. 11c) were rather similar. The signal at 2.039 could be assigned to O_2^- (23). A doublet superhyperfine structure due to O^- (23) was observed at 2.009 and 1.977. Further treatment in H_2 at 750°C for 1 h would result in the detection of a signal at 2.006 ascribable to trapped electrons (21) and the weakening of the doublet superhyperfine structure (Fig. 11d). After treatment in O_2 at 700°C for 30 min, the signal of trapped electron disappeared and those due to O_2^- and O^- species reappeared (Fig. 11e).

The EPR spectra of 30 mol% BaF_2/Y_2O_3 and 30 mol% $BaBr_2/Y_2O_3$ samples recorded after different treatments are shown in Fig. 12. When the samples were kept in air at 25°C, only O^- species were observed with g values at 2.014 and 1.975 (Figs. 12a and 12a′). After being treated in an O_2 flow at 700°C for 30 min, signals at 2.041, 2.023, and 1.975 (Fig. 12b) and 2.045, 2.021, and 1.977 (Fig. 12b′) were detected. Further treatment in a hydrogen flow at 700°C for 30 min led to the detection of trapped electrons with g tensors of 2.006 and 2.007, respectively, and the disappearance of all the other signals (Figs. 12c and 12c′). When the samples were treated progressively in O_2 at 700°C for 30 min, cooled in O_2 to 25°C, purged with C_2H_6 at 25°C and in C_2H_6 at 500°C for 30 min, the signal at $g = 1.975$ (Fig. 12d) and the signals at $g = 1.977$ and 2.021 (Fig. 12d′) decreased in intensity as compared, respectively, to those of Figs. 12b and 12b′. Raising the C_2H_6 treatment temperature to 640°C weakened the intensities of the signals at $g = 2.023$ and

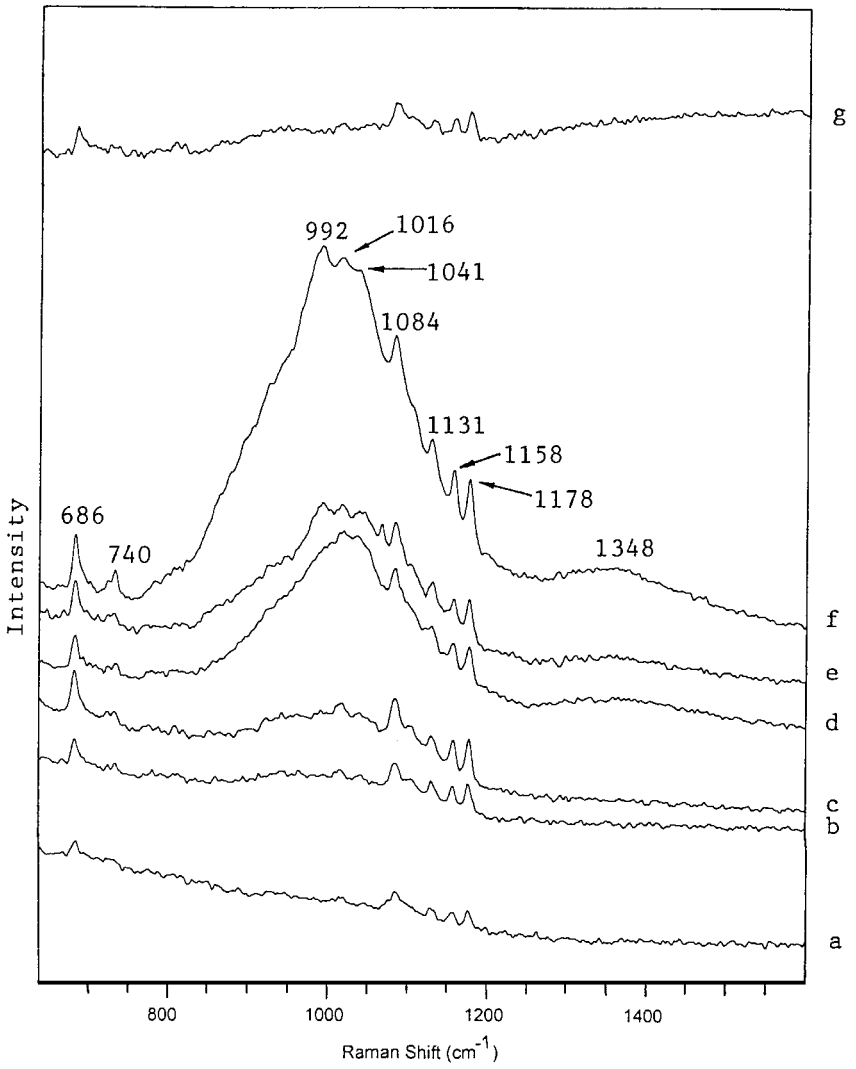

FIG. 10. Laser Raman spectra of a 30 mol% $BaCl_2/Y_2O_3$ sample when it was treated: (a) in air at room temperature, (b) then in N_2 at 600°C for 20 min, (c) then in O_2 at 600°C for 30 min, (d) then in O_2 at 640°C for 30 min, (e) then in $C_2H_6/O_2/N_2$ (molar ratio, 2/1/3.7) at 640°C for 45 min, (f) then in O_2 at 750°C for 30 min, and (g) then in C_2H_6 at 640°C for 30 min.

1.975 (Fig. 12e), whereas the signal at $g = 2.021$ was eliminated and the signal intensity at $g = 1.977$ (Fig. 12e′) was diminished. After further treatment in C_2H_6 at 700°C for 30 min, the two samples showed strong signals of trapped electrons at $g = 2.006$ (Fig. 12f) and at $g = 2.007$ (Fig. 12f′) and no oxygen species were detected. With the treatment in $C_2H_6/O_2/N_2$ (molar ratio = 2/1/3.7) at 640°C for 30 min, the 30 mol% $BaBr_2/Y_2O_3$ and 30 mol% BaF_2/Y_2O_3 samples showed spectra (Figs. 12g and 12g′) quite similar to those treated in O_2 at 700°C for 30 min (Figs. 12b and 12b′) except for a relatively weaker intensity at $g = 1.975$ and $g = 1.977$, respectively. As for the 30 mol% BaO/Y_2O_3 catalyst, treatment in O_2 at 640°C for 30 min would give rise to a strong signal at $g = 1.976$ and weak signals at $g = 2.044$ and 2.022 (Fig. 12h), indicating that a large amount of O^- species and a small amount of O_2^- species were formed.

Figure 13 shows the EPR spectra of a 30 mol% $BaCl_2/Y_2O_3$ catalyst treated in different atmospheres at various temperatures. When the sample was kept in air at 25°C, only O^- species was detectable with g values at 2.015 and 1.974 (Fig. 13a). When the sample was treated in O_2 at 700°C for 30 min, signals at 2.043, 2.034, 2.022, and 1.974 were observed (Fig. 13b). Further treatment in H_2 at 500°C caused all the signals to reduce in intensity (Fig. 13c). After treatment in H_2 at 700°C for 30 min, the signal centered at 2.006 due to trapped electrons appeared and all the previously observed signals of oxygen adspecies disappeared (Fig. 13d). For a 30 mol% $BaCl_2/Y_2O_3$ sample first treated in O_2 at 700°C for 30 min and then cooled in O_2 to 25°C and purged with C_2H_6 at 25°C, the signals at 2.034 and 2.022 changed little, whereas the signal at 1.974 increased in intensity (Fig. 13e). Further treatment in C_2H_6 at 500°C for

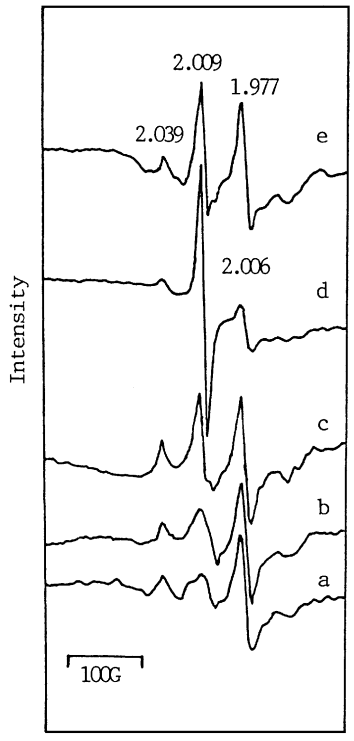

FIG. 11. EPR spectra of undoped Y_2O_3: (a) in air at room temperature, (b) then in H_2 at 500°C for 1 h, (c) then in H_2 at 700°C for 1 h, (d) then in H_2 at 750°C for 1 h, and (e) then in O_2 at 700°C for 30 min.

30 min caused the signal intensity at 1.974 to increase significantly and the signal intensity at 2.022 to decrease slightly (Fig. 13f). The intensities of the signals at 2.022 and 1.974 decreased obviously after further C_2H_6 treatment at 640°C (Fig. 13g). After being treated in C_2H_6 at 700°C for 30 min, the sample showed a strong signal of trapped electrons at 2.006 and no signals due to oxygen adspecies could be observed (Fig. 13h). After treatment in $C_2H_6/O_2/N_2$ (molar ratio = 2/1/3.7) at 640°C for 30 min, the sample showed a spectrum rather similar to that of Fig. 13b except that the signal at 1.974 had lower intensity (Fig. 13i).

DISCUSSION

Catalytic Performance

From Figs. 1a–1c, one can observe that at a 30 mol% loading of BaO, $BaCl_2$, or $BaBr_2$ in the BaO- or BaX_2 (X = Cl and Br)-promoted Y_2O_3 catalysts, the C_2H_4 yield was at its maximum. After 40 h of on-stream ODE reaction, the 30 mol% BaO/Y_2O_3 and 30 mol% $BaBr_2/Y_2O_3$ catalysts degraded, whereas the 30 mol% $BaCl_2/Y_2O_3$ catalyst showed a sustainable activity (Figs. 2a–2c). In the space velocity study (Fig. 3), with increasing space velocity, the C_2H_6 conversion and CO_x selectivity decreased while the C_2H_4 selectivity increased. Over a 30 mol% $BaCl_2/Y_2O_3$ catalyst well dispersed in quartz sand, we made the same observation. This implied that the problem of hot spots was not serious over 30 mol% $BaCl_2/Y_2O_3$.

As shown in Table 1, single-component barium oxide or barium halides showed poor C_2H_6 conversion and C_2H_4 yield at 640°C. The undoped Y_2O_3 catalyst gave a C_2H_4 yield of 36.7% and the C_2H_4 selectivity was 59.0%. With the addition of 30 mol% MO (M = Mg, Ca, and Sr) to

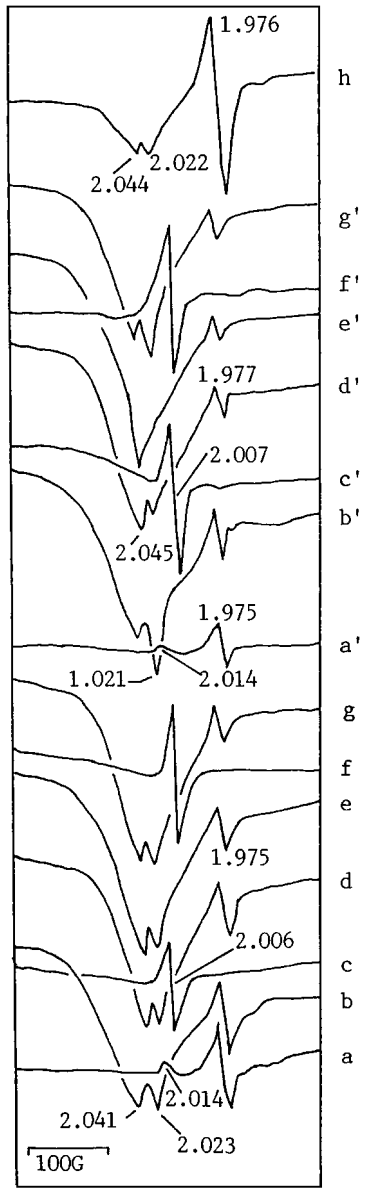

FIG. 12. EPR spectra of 30 mol% BaF_2/Y_2O_3 (a–g) and 30 mol% $BaBr_2/Y_2O_3$ (a′–g′): (a, a′) in air at room temperature; (b, b′) then in O_2 at 700°C for 30 min; (c, c′) then in H_2 at 700°C for 30 min; (d, d′) first in O_2 at 700°C for 30 min, then cooled down in O_2 to 25°C, and then purged with C_2H_6 at 25°C for 30 min and then in C_2H_6 at 500°C for 30 min; (e, e′) then in C_2H_6 at 640°C for 30 min; (f, f′) then in C_2H_6 at 700°C for 30 min; (g, g′) then in $C_2H_6/O_2/N_2$ (molar ratio, 2/1/3.7) at 640°C for 30 min. (h) An EPR spectrum of 30 mol% BaO/Y_2O_3 after treatment in O_2 at 640°C for 30 min.

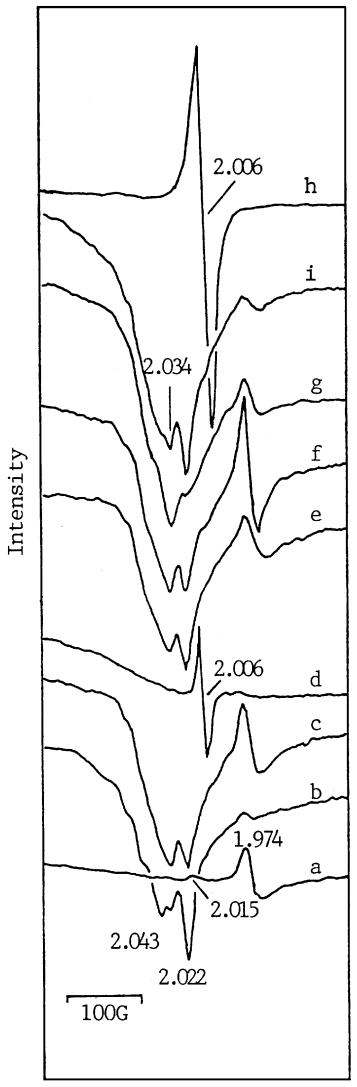

FIG. 13. EPR spectra of 30 mol% $BaCl_2/Y_2O_3$: (a) in air at 25°C; (b) then in O_2 at 700°C for 30 min, (c) then in H_2 at 500°C for 30 min, (d) then in H_2 at 700°C for 30 min, (e) first in O_2 at 700°C for 30 min and then cooled down in O_2 to 25°C and in C_2H_6 at 25°C for 30 min, (f) then in C_2H_6 at 500°C for 30 min, (g) then in C_2H_6 at 640°C for 30 min, (h) then in C_2H_6 at 700°C for 30 min, and (i) then in $C_2H_6/O_2/N_2$ (molar ratio, 2/1/3.7) at 640°C for 30 min.

Y_2O_3, C_2H_4 selectivity enhanced obviously, whereas C_2H_6 conversion decreased. The 30 mol% BaO/Y_2O_3 catalyst showed 62.9% C_2H_6 conversion, 68.1% C_2H_4 selectivity, and 42.8% C_2H_4 yield at 640°C. The performance of a 30 mol% $BaCO_3/Y_2O_3$ catalyst is inferior to pure Y_2O_3. Among the BaX_2 (X = F, Cl, and Br)-modified Y_2O_3 catalysts, 30 mol% $BaCl_2/Y_2O_3$ is the best, giving a C_2H_6 conversion of 72.1%, a C_2H_4 selectivity of 73.6%, and a respectable C_2H_4 yield of 53.1% at 640°C. The 30 mol% $BaBr_2/Y_2O_3$ catalyst showed a C_2H_4 selectivity of 77.7% and a C_2H_4 yield of 44.4% at 640°C. The C_2H_4 selectivity of 30 mol% BaF_2/Y_2O_3 is similar to that of 30 mol% $BaCl_2/Y_2O_3$ but the C_2H_6 conversion of the former is lower than that of the latter. With both C_2H_4 selectivity and C_2H_6 conversion being taken into consideration, one can conclude that the catalytic performance increased in the order 30 mol% $BaCO_3/Y_2O_3 <$ 30 mol% $MgO/Y_2O_3 <$ 30 mol% $CaO/Y_2O_3 \approx$ 30 mol% $SrO/Y_2O_3 < Y_2O_3 <$ 30 mol% $BaF_2/Y_2O_3 <$ 30 mol% $BaO/Y_2O_3 <$ 30 mol% $BaBr_2/Y_2O_3 <$ 30 mol% $BaCl_2/Y_2O_3$.

From Table 2, one can observe that, with the increase in C_2H_4 selectivity due to temperature rise, O_2 conversion increased over the Y_2O_3, 30 mol% BaO/Y_2O_3, 30 mol% BaF_2/Y_2O_3, and 30 mol% $BaBr_2/Y_2O_3$ catalysts; whereas over the 30 mol% $BaCl_2/Y_2O_3$ catalyst, O_2 conversion first decreased and then increased. The oxidation of C_2H_6 involves several reactions:

$$C_2H_6 + (1/2)O_2 \rightarrow C_2H_4 + H_2O \quad [1]$$

$$C_2H_6 + (5/2)O_2 \rightarrow CO + 3H_2O \quad [2]$$

$$C_2H_6 + (7/2)O_2 \rightarrow 2CO_2 + 3H_2O \quad [3]$$

$$C_2H_6 + O_2 \rightarrow CO + CH_4 + H_2O. \quad [4]$$

Compared to reactions [2], [3], and [4], reaction [1] consumes less oxygen. C_2H_6 conversion and C_2H_4 selectivity increase simultaneously if reactions [2], [3], and [4] are suppressed. An enhancement in C_2H_4 selectivity signals the predominance of reaction [1] in which a smaller amount of O_2 can convert relatively more C_2H_6. As a result, when O_2 conversion dropped, C_2H_6 conversion and C_2H_4 selectivity increased concurrently over the 30 mol% $BaCl_2/Y_2O_3$ catalyst.

After investigating a number of chloride-promoted oxide catalysts, Burch *et al.* (33) suggested that the presence of chloride ions on the catalyst surface could eliminate the sites for complete oxidation and create new active sites for the selective oxidation of ethane to ethene. By using ^{13}C-labeled C_2H_4 and C_2H_6, Lunsford *et al.* (34) found that at or above 650°C C_2H_4 was the major source for CO_x formation. In other words, if the deep oxidation of C_2H_4 can be hindered, C_2H_4 selectivity would be enhanced. As shown in Table 3, by doping Y_2O_3 with BaO or BaX_2 (X = F, Cl, and Br), the deep oxidation of C_2H_4 was inhibited to various extents. The three halide-modified Y_2O_3 catalysts showed low C_2H_4 conversions in the C_2H_4 oxidation reaction and high C_2H_4 selectivities in the ODE reaction. A similar effect was also observed on the $BaBr_2$-modified Ho_2O_3 catalyst (22). Therefore, we conclude that the addition of barium halides can reduce the deep oxidation of C_2H_4 formed in the ODE reaction and thus improve significantly the C_2H_4 selectivity.

Influence of Calcination Temperature and Halogen on Catalytic Activity

The activity data listed in Table 4 illustrate that a 30 mol% BaX_2/Y_2O_3 (X = Cl and Br) catalyst calcined at 900°C performed better than a similar catalyst calcined at 800 or 1000°C, whereas a 30 mol% BaF_2/Y_2O_3 catalyst calcined at

800 or 900°C was a little inferior to that calcined at 1000°C. The concentration and distribution of defects formed in a solid material prepared by solid reaction are closely related to the calcination temperature. West (35) pointed out that solid state reactions between two powders can be sped up in the presence of a small amount of liquid phase that acts as a medium for the transport of matter; an excessive amount of the liquid phase, nevertheless, is obviously undesirable. It has been observed that there were ionic exchanges between the BaX_2 and Y_2O_3 phases in a BaX_2/Y_2O_3 catalyst (20). The size of Ba^{2+} ion (radius, 1.43 Å) is larger than that of Y^{3+} ion (0.88 Å). If a certain amount of Ba^{2+} ions entered into the lattice of Y_2O_3, due to the fact that Ba^{2+} is larger and inducing smaller coulombic forces, the occupancy of Y_2O_3 lattice points by Ba^{2+} ions would cause the Y_2O_3 lattice to expand. Along with the infiltration of Ba^{2+} ions, a certain amount of O^{2-} ions inside the Y_2O_3 lattice could be replaced by the incoming X^- ions, and the Y_2O_3 lattice would enlarge even more. Similar ionic exchanges could take place in the BaX_2 lattice. The incorporation of a certain amount of Y^{3+} ions into the BaX_2 lattice caused it to contract. The radii of O^{2-}, F^-, Cl^-, and Br^- ions are 1.40, 1.38, 1.81, and 1.95 Å, respectively. Along with the incorporation of Y^{3+} ions, a certain amount of X^- ions inside the BaX_2 lattice could be displaced by the incoming O^{2-} ions, and for $BaCl_2$ and $BaBr_2$, the BaX_2 lattice would contract even more. The extent of such ionic substitutions would determine the defect density and hence the catalytic activity. As shown in Table 4, the enlargement of cubic Y_2O_3 and the contraction of BaX_2 were the most significant when the catalyst was calcined at 900°C for the BaX_2 ($X = $ Cl and Br)-modified Y_2O_3 catalysts. The melting points of Y_2O_3 and BaX_2 ($X = $ F, Cl, and Br) are ca. 2439, 1368, 963, and 857°C, respectively. It is apparent that ionic exchanges of the Ba^{2+} and Y^{3+} and the X^- ($X = $ Cl and Br) and O^{2-} ions between the BaX_2 and Y_2O_3 phases proceeded more readily at 900°C than at 800°C, whereas those of the Ba^{2+} and Y^{3+} and the F^- and O^{2-} ions between the BaF_2 and Y_2O_3 phases were more favorable at 1000°C than at or below 900°C. For 30 mol% BaF_2/Y_2O_3, with the increase in calcination temperature from 800 to 1000°C (which is much lower than the melting point of BaF_2), the enlargement of the Y_2O_3 lattice, and the contraction of the BaF_2 lattice were not significant; i.e., defect formation was insignificant. A 30 mol% BaX_2 ($X = $ Cl and Br)/Y_2O_3 sample calcined at 1000°C (which is higher than the melting points of BaX_2), however, showed the smallest a_0 value of Y_2O_3 and the largest a, b, and c values of BaX_2; the X composition and surface area were the lowest among the three calcined samples. We suggest that due to the losses of Cl and Br at such a high temperature, defect formation was less favorable. Both the reductions in defect density (as indicated by the a_0 value of Y_2O_3 as well as the a, b, and c values of BaX_2) and surface area (most likely due to sintering) caused the catalytic activity to decrease (Table 4). Generally speaking, the more the defects in a catalyst the better will be the catalytic performance. As shown in Table 4, The best activity was achieved over the catalyst that showed the largest expansion of the Y_2O_3 lattice and the biggest contraction of BaX_2 lattice in the 30 mol% BaX_2-modified Y_2O_3 catalysts.

The effects of halogen present either in the form of a halide component or as a volatile halogenated compound in the reactant feed on the performance of catalysts for the OCM or ODE reaction have been intensely investigated by many researchers (33, 36–46). It is generally accepted that the presence of halogen could enhance significantly the CH_4 conversion and C_{2+} selectivity in the OCM reaction as well as the C_2H_6 conversion and C_2H_4 selectivity in the ODE reaction. Osada *et al.* (47) detected the lattice distortions of yttrium oxide induced by the infiltration of Ca^{2+} into the Y_2O_3 lattice in the binary oxide Y_2O_3–CaO catalyst. Kaminsky *et al.* (48) proposed that the substitution of Ba^{2+} into Y^{3+} lattice sites in the Ba-doped Y_2O_3 catalyst could create active (charge-deficient oxygen) sites. Erarslanoglu *et al.* (49) reported that the incorporation of Sr^{2+} cations into the Y_2O_3 lattice led to the formation of defective structure. In our previous studies (21–24, 50), we proposed that the presence of MO or MX_2 ($M = $ Sr and Ba; $X = $ F, Cl, and Br) in rare earth oxides caused the rare earth oxide lattices to enlarge and the MO or MX_2 lattice to contract due to partial ionic exchanges between phases. In the case of the BaX_2-promoted Y_2O_3 catalysts, if ionic exchange has occurred, the formation of O^- centers and trapped electrons may be expected (24, 50). Taking into account the sizes of O^{2-}, F^-, Cl^-, and Br^- ions, the extent of ionic exchange between O^{2-} and X^- ions followed the order of $F^- > Cl^- > Br^-$. Under the influence of calcination temperature, the sequence was actually $Cl^- > Br^- > F^-$ in the present study. The generation of lattice defects is favorable for the activation of gaseous oxygen molecules. The increase in the amount of desorbed O_2 in O_2-TPD studies after the addition of BaX_2 to Y_2O_3 is supporting evidence for this viewpoint. Oxygen molecules could pick up trapped electrons to form O_2^-, O_2^{2-}, O^-, O_3^-, or even O^{2-} adspecies, which are active in the ODE reaction (22–24, 51–55). After making detailed investigations on various oxygen species on/in MgO-based catalysts, Lunsford and co-workers (51–55) concluded that the reactivity of these mono- and polynuclear oxygen species with C_2H_6 followed the sequence of $O^- \gg O_3^- \gg O_2^{2-} > O_2^- > O^{2-}$. As for the BaX_2/Y_2O_3 catalysts, the generation of O^- centers and trapped electrons enhanced the catalytic behaviors.

It should be noted that besides the defective structures, good performances of the BaX_2-modified Y_2O_3 catalysts might be associated with the surface and bulk halogen compositions as well as the surface basicity and surface area of the catalysts. From Table 4, one can see that the surface and bulk Cl^- compositions of 30 mol% $BaCl_2/Y_2O_3$ were rather

similar, indicative of a uniform dispersion of Cl^- ions in the catalyst. The introduction of halides to Y_2O_3 would lead to a lowering of surface basicity, reducing the deep oxidation of ethene as a result (47). In the OCM reaction, the decrease in surface area of a catalyst would lead to a rise in C_2 selectivity (56, 57). From the activity data in Table 4, one can observe that with the decrease in surface area, the C_2H_4 selectivity rises. Therefore, we suggest that a uniform halide distribution in the catalyst and a suitable surface basicity appear to be favorable for the improvement of catalytic activity.

CO_2 Poisoning

As pointed out by Lunsford *et al.* (2, 3), a Li/MgO catalyst used for the ODE reaction suffered from CO_2 poisoning. However, with the introduction of Cl^- ions to the catalyst, CO_2 poisoning could be suppressed. The extent of CO_2 poisoning depends upon the basicity of the catalyst surface. If the surface basicity of a catalyst is high, strong CO_2 adsorption would take place, leading to a low catalytic activity (2, 3). Previously, we have suggested that a medium-strong basicity was favorable for the formation of C_2H_4 over a 50 mol% $BaBr_2/Ho_2O_3$ catalyst (22). It could be seen (Figs. 2a and 2c) that over the 30 mol% BaO/Y_2O_3 and 30 mol% $BaBr_2/Y_2O_3$ catalysts, with the increase in reaction time, C_2H_6 conversion, C_2H_4 selectivity, and C_2H_4 yield decreased continuously. After 40 h of on-stream ODE reaction, both catalysts showed performance only slightly better than that of a 30 mol% $BaCO_3/Y_2O_3$ catalyst. We conclude that during the ODE reaction, the BaO on the surface of 30 mol% BaO/Y_2O_3 was transformed into $BaCO_3$ (Table 6); in the 30 mol% $BaBr_2/Y_2O_3$ catalyst, due to Br leaching, a certain amount of $BaCO_3$ was also formed (Table 6). The XRD results indicated that after 40 h of the reaction, the signal intensity of the $BaCO_3$ phase was medium in 30 mol% BaO/Y_2O_3, weak in 30 mol% BaF_2/Y_2O_3, very weak in 30 mol% $BaCl_2/Y_2O_3$, and medium in 30 mol% $BaBr_2/Y_2O_3$. In other words, the extent of CO_2 adsorption over these catalysts followed the order of 30 mol% $BaO/Y_2O_3 \approx$ 30 mol% $BaBr_2/Y_2O_3 >$ 30 mol% $BaF_2/Y_2O_3 \gg$ 30 mol% $BaCl_2/Y_2O_3$. The first three catalysts were poisoned rather readily by CO_2 whereas the 30 mol% $BaCl_2/Y_2O_3$ catalyst was quite resistant to CO_2 poisoning.

From Table 5, one can observe that with the extension of reaction time, the 30 mol% BaO-modified Y_2O_3 catalyst deteriorated rapidly, the 30 mol% BaF_2/Y_2O_3 and 30 mol% $BaBr_2/Y_2O_3$ catalysts degraded gradually, and the 30 mol% $BaCl_2/Y_2O_3$ catalyst showed stable performance. These results provided direct supporting evidences that the 30 mol% $BaCl_2/Y_2O_3$ catalyst was resistant to CO_2 poisoning whereas the 30 mol% BaO/Y_2O_3, 30 mol% BaF_2/Y_2O_3, and 30 mol% $BaBr_2/Y_2O_3$ catalysts were prone to CO_2 poisoning.

After 40 h of reaction, the surface area of 30 mol% $BaCl_2/Y_2O_3$ decreased only by ca. 3%, whereas the surface areas of 30 mol% BaO/Y_2O_3, 30 mol% BaF_2/Y_2O_3, and 30 mol% $BaBr_2/Y_2O_3$ decreased substantially by ca. 38, 46, and 33%, respectively (Table 6). We consider that the decrease in surface area might be assoiated with halogen leaching and the formation of the $BaCO_3$ phase. From Table 7, the distributions of Cl^- ions on the surface and in the bulk of 30 mol% $BaCl_2/Y_2O_3$ were rather uniform and the surface and bulk Cl^- concentrations did not alter significantly after 40 h of reaction. In the 30 mol% BaF_2/Y_2O_3 catalyst, the surface composition of F^- ions decreased by ca. 22% whereas the bulk composition decreased only slightly. As for the 30 mol% $BaBr_2/Y_2O_3$ catalyst, the bulk composition of Br^- ions decreased by ca. 52% whereas the Br surface composition increased by ca. 3%. These results suggested that in the BaX_2/Y_2O_3 catalysts, the Cl^- ions were rather stable and were evenly distributed; the F^- ions dwelt in the bulk whereas the Br^- ions leached. Similar tendencies of halide ion diffusion were also observed in the studies of BaX_2/Ho_2O_3 catalysts (22).

In the CO_2-TPD studies (Fig. 4), Y_2O_3 showed moderate CO_2 desorption at temperatures below 400°C and substantial CO_2 desorption began at ca. 744°C, indicating that most of the adsorption sites were strongly basic. Compared to a fresh 30 mol% BaO/Y_2O_3 sample (Fig. 4c), the CO_2 desorption peaks at temperatures below 200°C and above 600°C were larger than those obtained over a used sample (Fig. 4c′) and the threshold temperature (ca. 661°C) for large CO_2 desorption over the used sample was lower than that (ca. 705°C) over the fresh one. It is worth pointing out that the CO_2-TPD profile of the used 30 mol% BaO/Y_2O_3 sample was rather similar to that of a 30 mol% $BaCO_3/Y_2O_3$ sample (Fig. 4b). It demonstrated that after 40 h of ODE reaction, the 30 mol% BaO/Y_2O_3 catalyst was indeed transformed to a material somewhat like a 30 mol% $BaCO_3/Y_2O_3$ catalyst due to CO_2 adsorption. As for the 30 mol% BaF_2/Y_2O_3 catalyst, the used sample (Fig. 4d′) showed a large CO_2 desorption peak at a threshold temperature of ca. 630°C and the overall CO_2 desorption over the used catalyst was much larger than that observed over the fresh one (Fig. 4d). For 30 mol% $BaBr_2/Y_2O_3$, the amounts of CO_2 desorbed at temperatures below 300°C and above 400°C over the used sample (Fig. 4f′) were much larger than that desorbed over the fresh one (Fig. 4f), and the desorption temperatures shifted toward higher temperatures. Both 30 mol% BaF_2/Y_2O_3 and 30 mol% $BaBr_2/Y_2O_3$ catalysts were prone to CO_2 poisoning. For the 30 mol% $BaCl_2/Y_2O_3$ catalyst, however, although the temperatures of CO_2 desorption changed slightly, the extents of CO_2 desorption were similar over the fresh (Fig. 4e) and the used (Fig. 4e′) samples. It indicated that the 30 mol% $BaCl_2/Y_2O_3$ catalyst was resistant to CO_2 poisoning. The stable performance of the $BaCl_2$-doped Y_2O_3 catalyst in a period of

40 h ODE reaction confirmed this point. Therefore, one can conclude that the gradual decrease in catalytic performance over the 30 mol% BaO/Y_2O_3, 30 mol% BaF_2/Y_2O_3, and 30 mol% $BaBr_2/Y_2O_3$ catalysts was due to CO_2 poisoning (and halogen leaching as well for the latter two). The 30 mol% $BaCl_2/Y_2O_3$ was resistant to CO_2 poisoning, in good agreement with the viewpoint that Cl^- ions in catalyst can suppress CO_2 poisoning (2).

Active Oxygen Species

As observed in the O_2-TPD studies (Fig. 5), with the addition of BaO, $BaCO_3$, or BaX_2 ($X = F$, Cl, and Br) to Y_2O_3, the amount of oxygen desorbed from the catalysts increased considerably and followed the order of 30 mol% $BaO/Y_2O_3 >$ 30 mol% $BaCO_3/Y_2O_3 >$ 30 mol% $BaCl_2/Y_2O_3 >$ 30 mol% $BaBr_2/Y_2O_3 >$ 30 mol% $BaF_2/Y_2O_3 >$ undoped Y_2O_3. Relatively speaking, the first two catalysts exhibited larger O_2 desorptions and showed lower C_2H_4 selectivities in the ODE reaction (Tables 1 and 2), indicating that a high concentration of surface oxygen adspecies favored the deep oxidation reactions. The used 30 mol% $BaCl_2/Y_2O_3$ catalyst showed an O_2 desorption peak (Fig. 5d′) rather similar to that of a fresh sample, indicating that the 30 mol% $BaCl_2/Y_2O_3$ catalyst was rather intact in the ODE reaction. The amount of oxygen in these catalysts reducible by H_2 followed a sequence similar to that of oxygen desorption. Based on the results of TPR studies (Fig. 6), the amount of oxygen reduced by H_2 increased with the addition of BaO or BaX_2, and the order is 30 mol% $BaO/Y_2O_3 >$ 30 mol% $BaCl_2/Y_2O_3 >$ 30 mol% $BaBr_2/Y_2O_3 >$ 30 mol% $BaF_2/Y_2O_3 >$ undoped Y_2O_3. It is clear that the addition of promoters such as BaO and BaX_2 to Y_2O_3 could enhance significantly the extent of oxygen adsorption. In other words, the ability of activating gaseous O_2 molecules was enhanced via the modification of Y_2O_3 by BaO or BaX_2.

Eysel and Thym (27) suggested that the vibrational frequency for surface peroxide (O_2^{2-}) lies in the region of 730–950 cm^{-1}. Valentine (58) suggested that perturbed intermediate oxygen species O_2^{n-} ($1 < n < 2$) should give rise to bands in the 900–1100 cm^{-1} region. In one of our previous studies (26), we reported that the Raman bands of BaO_2 and CsO_2 at 840 and 1122 cm^{-1} were corresponding to O_2^{2-} and O_2^-, respectively. We also suggested that Raman bands within the 1200–1452 cm^{-1} range could be assigned to $O_2^{\delta-}$ ($0 < \delta < 1$) and the band at ca. 668 cm^{-1} to sublayer O_2^{2-} species. Smith (59) observed a vibrational frequency around 1550 cm^{-1} that was assigned to neutral O_2. By treating the 30 mol% BaO/Y_2O_3 sample in O_2 at 800°C for 20 min (Fig. 7a), Raman bands were observed at 694 and 1062 cm^{-1} (CO_3^{2-}), 842 cm^{-1} (O_2^{2-}), 1026 cm^{-1} (O_2^{n-} ($1 < n < 2$)), and ca. 1387 cm^{-1} ($O_2^{\delta-}$ ($0 < \delta < 1$)). Further treatment in N_2 at temperatures from 500 to 800°C caused the Raman bands to broaden and to reduce in intensity (Figs. 7b–7d). Little change was observed when the sample was treated in C_2H_6 at 640°C for 30 min (Fig. 7e). However, after C_2H_6 treatment at 700°C for 30 min, only weak signal at ca. 694 and 1055 cm^{-1} (CO_3^{2-}) could be observed, indicating that the O_2^{2-}, $O_2^{\delta-}$, and O_2^{n-} species reacted with ethane (Fig. 7f). Further treatment in C_2H_6 at 750°C for 30 min (Fig. 7g) eliminated all the Raman signals, indicating that above 750°C, the CO_3^{2-} species decomposed. The signals of all the oxygen adspecies reappeared when the sample was treated in O_2 at 800°C for 30 min (Fig. 7h). Based on these Raman results, we conclude that the O_2^{2-}, $O_2^{\delta-}$, O_2^{n-} species are active for the conversion of ethane. For the fresh 30 mol% BaF_2/Y_2O_3 and 30 mol% $BaBr_2/Y_2O_3$ catalysts, with the rise in O_2 treatment temperature from 640 to 750°C, more dioxygen O_2^{n-}, O_2^{2-}, and $O_2^{\delta-}$ species were formed (Figs. 8a and 8b and 9a and 9b). The introduction of a reactant mixture to the catalysts at 640°C led to the decrease in the amount of the dioxygen species (Figs. 8c and 9c), indicating that dioxygen species were involved in C_2H_6 conversion. Further treatment in C_2H_6 at the same temperature caused the dioxygen signals to disappear completely (Figs. 8d and 9d), a clear indication of dioxygen species being active in C_2H_6 activation. Subsequent treatment of the samples in O_2 at 750°C (Figs. 8e and 9e) restored the O_2^{n-}, O_2^{2-}, and $O_2^{\delta-}$ species. These Raman results demonstrated that O_2^{n-}, O_2^{2-}, and $O_2^{\delta-}$ species over the 30 mol% BaF_2- and $BaBr_2$-doped Y_2O_3 catalysts were actively involved in the conversion of ethane. As for a fresh 30 mol% $BaCl_2/Y_2O_3$ catalyst (Fig. 10a), treatment in N_2 at 600°C for 20 min (Fig. 10b) did not bring about any significant changes. Treatments in O_2 for 30 min at 600 and 640°C (Figs. 10c and 10d) intensified the Raman signals within the 900–1050 cm^{-1} range, indicating that O_2^{n-} and/or O_2^{2-} (18, 27, 58) species were formed; in the meanwhile, the bands at ca. 1068 and 1084 cm^{-1} corresponding to O_2^{n-} species (58) and the bands at 1131, 1158, and 1178 cm^{-1} corresponding to O_2^- species (26, 28–32) increased only slightly in intensity, and a new band centered at ca. 1340 cm^{-1} (Fig. 10d) that could be ascribed to $O_2^{\delta-}$ (26) appeared. After further treatment of this sample in $C_2H_6/O_2/N_2$ (molar ratio, 2/1/3.7) at 640°C for 45 min (Fig. 10e), the signals of the O_2^- species remained almost unaltered, whereas the bands of the O_2^{n-} and/or O_2^{2-} species decreased obviously in intensity, indicating that the O_2^{n-} and/or O_2^{2-} species had participated in the ODE reaction. Further treatment of the sample in O_2 at 750°C for 30 min resulted in signal recoveries of the O_2^{n-}, O_2^-, $O_2^{\delta-}$, and O_2^{2-} species (Fig. 10f). After treatment in C_2H_6 at 640°C for 30 min (Fig. 10g), only the O_2^- species (with signals at ca. 1131, 1158, and 1178 cm^{-1}) and the sublayer O_2^{2-} species (with signal at ca. 686 cm^{-1}) remained with diminished signals and all the other oxygen species disappeared, demonstrating that O_2^{n-}, $O_2^{\delta-}$, and O_2^{2-} species had been involved in the reaction of C_2H_6 conversion and that

these three dioxygen species were more reactive than O_2^- and sublayer O_2^{2-} species toward C_2H_6.

From the reactivities of the various oxygen species discussed above, we believe that under the reaction conditions adopted, O_2^{2-}, $O_2^{\delta-}$, and O_2^{n-} are more active than O_2^- and sublayer O_2^{2-}. In oxygen chemisorption, O^- and O_2^- adspecies are usually formed simultaneously and O^- could transform to O^{2-} and/or O_2^- under certain conditions (60). The EPR spectra of paramagnetic species O^- and O_2^- vary, depending upon the nature of the catalyst and treatment conditions. Wang and Lunsford (18) found that there was superoxide ion O_2^- with g components at 2.090, 2.079, 2.070, and 2.005 on a 7 wt% Li/MaO catalyst treated in 192 Torr of O_2 at 650°C for 1 h and quenched in liquid O_2 (−196°C). Previously, we reported the existence of O^- species with $g_\perp = 2.0000$ and $g_{//} = 1.9710$ (50) and O_2^- species with $g_\perp = 1.9731$ and $g_{//} = 2.0380$, 2.0319, 2.0179, and 2.0111 in a 20% SrF_2/SmOF catalyst (23). Among the various oxygen species, O^- is the most reactive with light hydrocarbons (51–55). From Fig. 11, one can realize that treating Y_2O_3 in air resulted in the detection of O_2^- and O^- species. Further reduction by H_2 at or above 500°C gave rise to trapped electrons. Both O_2^- and O^- species reappeared after O_2 treatment at 700°C. The Raman spectrum of Y_2O_3 also confirmed the existence of O_2^- species when the sample was exposed to O_2 at 800°C for 15 min and cooled to 25°C in O_2 (21). For the 30 mol% BaF_2/Y_2O_3 and 30 mol% $BaBr_2/Y_2O_3$ catalysts, only O^- species were present at room temperature (Figs. 12a and 12a′). O_2 treatment of the catalysts at 700°C resulted in the formation of O_2^- and O^- species (Figs. 12b and 12b′). When the two catalysts were reduced in H_2 (Figs. 12c and 12c′) or in C_2H_6 (Figs. 12f and 12f′) at 700°C, trapped electrons were generated. With the rise in treatment temperature in C_2H_6 from 500 to 640°C, the amounts of O^- and of the species with g = ca. 2.02 decreased (Figs. 12d, 12e, 12d′, and 12e′), indicating that both species had reacted with C_2H_6. Further treatment in a reactant mixture at 640°C resulted in the recovery of the O_2^- and O^- species (Figs. 12g and 12g′). For the 30 mol% BaO/Y_2O_3 catalyst, treatment in O_2 at 640°C enhanced the signal at $g = 1.976$ (Fig. 12h), indicating that there were large amount of O^- species on the surface. At 25°C, only O^- species were detected on a 30 mol% $BaCl_2/Y_2O_3$ catalyst (Fig. 13a). After treatment in O_2 at 700°C, both O^- and O_2^- species were observed (Fig. 13b). Trapped electrons could also be generated when the catalyst was reduced in H_2 (Fig. 13d) or in C_2H_6 (Fig. 13h) at 700°C. With the rise in C_2H_6 reduction temperature from 25 to 640°C (Figs. 13e–13g), the signal at $g = 2.022$ decreased gradually in intensity, indicating the corresponding species had reacted with C_2H_6; the signal with $g = 2.034$, however, altered only slightly in intensity, indicating the species were relatively less reactive with C_2H_6. The introduction of a reactant mixture at 640°C to the sample caused the reappearance of O_2^- species. One can observe from Fig. 13 that the intensity of the signal with $g = 1.974$ due to O^- species increased in intensity and the signal with $g = 2.022$ decreased when the sample was treated in C_2H_6 at 500°C (Fig. 13f). It indicated that at this temperature, a certain amount of O_2^- species was consumed while O^- species were generated. One can also realize that the signal intensities of O^- species on Y_2O_3 (Fig. 11) and on 30 mol% BaO/Y_2O_3 (Fig. 13) are stronger than those on 30 mol% BaX_2/Y_2O_3 (Figs. 12 and 13). In other words, there was a larger concentration of O^- species in Y_2O_3 and 30 mol% BaO/Y_2O_3 than in 30 mol% BaX_2/Y_2O_3. By comparing the relative Raman and EPR signal intensities of O_2^{n-} ($1 < n < 2$), O_2^{2-}, $O_2^{\delta-}$ ($0 < \delta < 1$), O_2^-, and O^- species on undoped Y_2O_3 as well as 30 mol% BaO- and BaX_2-promoted Y_2O_3, one may observe that the signal intensities of O_2^{n-}, O_2^{2-}, $O_2^{\delta-}$, and O_2^- decreased in the order of $BaCl_2/Y_2O_3 > BaBr_2/Y_2O_3 > BaF_2/Y_2O_3 > BaO/Y_2O_3$, whereas that of O^- increased in the sequence of $BaBr_2/Y_2O_3 < BaCl_2/Y_2O_3 < BaF_2/Y_2O_3 < BaO/Y_2O_3$. The C_2H_4 selectivity followed the order of $BaBr_2/Y_2O_3 > BaCl_2/Y_2O_3 > BaF_2/Y_2O_3 > BaO/Y_2O_3$ (Tables 1 and 2). Taking as well the C_2H_6 conversion into consideration, the catalytic performance followed the sequence of $BaCl_2/Y_2O_3 > BaBr_2/Y_2O_3 > BaF_2/Y_2O_3 > BaO/Y_2O_3$ (Tables 1 and 2). Therefore, we conclude that the O^- species are relatively more active for the deep oxidation of C_2H_4, whereas the O_2^{n-}, O_2^{2-}, $O_2^{\delta-}$, and O_2^- species are more selective for the oxidation of C_2H_6 to C_2H_4.

CONCLUSIONS

Based on the catalytic performances of the BaO- and BaX_2 (X = F, Cl, and Br)-modified Y_2O_3 catalysts, we know that the addition of BaO or BaX_2 to Y_2O_3 could significantly improve the C_2H_4 selectivity in the ODE reaction. It was observed that C_2H_4 deep oxidation was reduced over the BaX_2-modified Y_2O_3 catalysts. Over the 30 mol% $BaCl_2/Y_2O_3$ catalyst, a C_2H_6 conversion of 72.1%, a C_2H_4 selectivity of 73.6%, and a respectable C_2H_4 yield of 53.1% could be achieved at 640°C. We believe that the good performance of $BaCl_2/Y_2O_3$ might be closely related to the nature and density of the lattice defects induced by ionic exchanges between the BaX_2 and Y_2O_3 phases. The calcination temperature exerts direct influence on the defect concentration of catalysts. The enlargement of the cubic Y_2O_3 lattice and the contraction of the $BaCl_2$ lattice were the most pronounced when 30 mol% $BaCl_2/Y_2O_3$ was calcined at 900°C. The 30 mol% $BaCl_2/Y_2O_3$ catalyst was resistant to CO_2 poisoning and the Cl^- ions were uniformly distributed throughout the catalyst and were stable in 40 h of on-stream ODE reaction. The 30 mol% $BaBr_2/Y_2O_3$ catalyst, however, degraded due to Br leaching. The 30 mol% BaO/Y_2O_3 and 30 mol% BaX_2 (X = F and Br)/Y_2O_3 catalysts were readily poisoned by CO_2 adsorption and carbonate formation.

The addition of BaO and BaX_2 to Y_2O_3 could considerably enhance O_2 adsorption as well as activation. Based on the results of *in situ* Raman and EPR studies, we conclude that dioxygen adspecies such as O_2^{2-}, O_2^{n-} $(1 < n < 2)$, O_2^-, and $O_2^{\delta-}$ $(0 < \delta < 1)$ are active for the selective oxidation of C_2H_6 to C_2H_4, whereas monooxygen species such as O^- are relatively more active in the deep oxidation of C_2H_6.

ACKNOWLEDGMENTS

The project was fully supported by the Hong Kong Research Grants Council, UGC (HKBU 2050/97P). H. X. Dai and Y. W. Liu thank the HKBU for a Ph.D. studentship.

REFERENCES

1. Morales, E., and Lunsford, J. H., *J. Catal.* **118**, 255 (1989).
2. Conway, S. J., and Lunsford, J. H., *J. Catal.* **131**, 513 (1991).
3. Wang, D., Rosynek, M. P., and Lunsford, J. H., *J. Catal.* **151**, 155 (1995).
4. Conway, S. J., Wang, D. J., and Lunsford, J. H., *Appl. Catal.* **79**, L1 (1991).
5. Ruth, K., Kieffer, R., and Burch, R., *J. Catal.* **175**, 16 (1998).
6. Ruth, K., Burch, R., and Kieffer, R., *J. Catal.* **175**, 27 (1998).
7. Thorsteinson, E. M., Wilson, T. P., Young, F. G., and Kasai, P. H., *J. Catal.* **52**, 116 (1978).
8. Erdöhelyi, A., and Solymosi, F., *J. Catal.* **129**, 497 (1991).
9. Erdöhelyi, A., Máté, F., and Solymosi, F., *J. Catal.* **135**, 563 (1991).
10. Chang, Y. F., Somorjai, G. A., and Heinemann, H., *J. Catal.* **154**, 24 (1995).
11. Santamaría González, J., Martínez Lara, M., Bañares, M. A., Martínez Huerta, M. V., Rodríguez Castellón, E., Fierro, J. L. G., and Jiménez López, A., *J. Catal.* **181**, 280 (1999).
12. Sugiyama, S., Sogabe, K., Miyamoto, T., Hayashi, H., and Moffat, J. B., *Catal. Lett.* **42**, 127 (1996).
13. Kennedy, E. M., and Cant, N. W., *Appl. Catal.* **75**, 321 (1991).
14. Kennedy, E. M., and Cant, N. W., *Appl. Catal.* **87**, 171 (1992).
15. Luo, J. Z., and Wan, H. L., *Appl. Catal. A* **158**, 137 (1997).
16. Yi, G., Hayakawa, T., Anderson, A. G., Suzuki, K., Hamakawa, S., York, A. P. E., Shimizu, M., and Takehira, K., *Catal. Lett.* **38**, 189 (1996).
17. Ueda, W., Lin, S. W., and Tohmoto, I., *Catal. Lett.* **44**, 241 (1997).
18. Wang, J. X., and Lunsford, J. H., *J. Phys. Chem.* **90**, 5883 (1986).
19. Au, C. T., He, H., Lai, S. Y., and Ng, C. F., *J. Catal.* **163**, 399 (1996).
20. Au, C. T., Liu, Y. W., and Ng, C. F., *J. Catal.* **171**, 231 (1997).
21. Au, C. T., Zhou, X. P., Liu, Y. W., Ji, W. J., and Ng, C. F., *J. Catal.* **174**, 153 (1998).
22. Au, C. T., Chen, K. D., Dai, H. X., Liu, Y. W., Luo, J. Z., and Ng, C. F., *J. Catal.* **179**, 300 (1998).
23. Au, C. T., and Zhou, X. P., *J. Chem. Soc., Faraday Trans.* **93**(3), 485 (1997).
24. Au, C. T., Liu, Y. W., and Ng, C. F., *J. Catal.* **176**, 365 (1998).
25. Wells, A. F., "Structural Inorganic Chemistry," 5th ed. Oxford Univ. Press, Oxford, 1984.
26. Au, C. T., Zhou, X. P., and Wan, H. L., *Catal. Lett.* **40**, 101 (1996).
27. Eysel, H. H., and Thym, S., *Z. Anorg. Allg. Chem.* **411**, 97 (1975).
28. Li, C., Domen, K., Manuya, K., and Onishi, T., *J. Am. Chem. Soc.* **111**, 356 (1989).
29. Metcalfe, A., and Udesgankar, S., *J. Chem. Soc., Faraday Trans. I* **76**, 630 (1980).
30. Gland, J. L., Sexton, B. A., and Fisher, G. B., *Surf. Sci.* **95**, 587 (1980).
31. Che, M., and Tench, J. E., *Adv. Catal.* **33**, 1 (1983).
32. Zecchina, A., Spoto, G., and Coluccia, S., *J. Mol. Catal.* **14**, 351 (1982).
33. Burch, R., Crabb, E. M., Squire, G. D., and Tsang, S. C., *Catal Lett.* **2**, 249 (1989).
34. Wang, D. J., Rosynek, M. P., and Lunsford, J. H., *J. Phys. Chem.* **98**, 8371 (1994).
35. West, A. R., "Solid State Chemistry and Its Applications." Courier International Ltd., Great Britain, 1990.
36. Maitra, A. M., *Appl. Catal. A* **104**, 11 (1993).
37. Burch, R., Squire, G. D., and Tsang, S. C., *Appl. Catal.* **46**, 69 (1989).
38. Baldwin, T. R., Burch, R., Grabb, E. M., Squire, G. D., and Tsang, S. C., *Appl. Catal.* **56**, 219 (1989).
39. Sugiyuma, S., Matsumura, Y., and Moffat, J. B., *J. Catal.* **139**, 338 (1993).
40. Voyatzis, R., and Moffat, J. B., *J. Catal.* **142**, 45 (1993).
41. Thomas, J. M., Ueda, W., Williams, J., and Harris, K. D. M., *Faraday Discuss. Chem. Soc.* **87**, 33 (1989).
42. Khan, A. Z., and Ruckenstein, E., *Catal. Lett.* **13**, 95 (1992).
43. Lunsford, J. H., Hinson, P. G., Rosynek, M. P., Shi, C., Xu, M., and Yang, X., *J. Catal.* **147**, 301 (1994).
44. Otsuka, K., Hatano, M., and Komatsu, T., *Stud. Surf. Sci. Catal.* **369**, 383 (1988).
45. Fujimoto, K., Hashimoto, S., Asami, K., Omata, K., and Tominaga, H., *Appl. Catal.* **50**, 223 (1989).
46. Zhou, X. P., Zhang, W. D., Wan, H. L., and Tsai, K. R., *Catal. Lett.* **21**, 113 (1993).
47. Osada, Y., Koike, S., Fukushima, T., Ogasawara, S., Shikada, T., and Ikariya, T., *Appl. Catal.* **59**, 59 (1990).
48. Kaminsky, M. P., Zajac, G. W., Campuzano, J. C., Faiz, M., Beaulaige, L., Gofron, K., Jenning, G., Yao, J. M., and Saldin, D. K., *J. Catal.* **136**, 16 (1992).
49. Erarslanoglu, Y., Onal, I., Dogu, T., and Senkan, S., *Appl. Catal. A* **145**, 75 (1996).
50. Au, C. T., and Zhou, X. P., *J. Chem. Soc. Faraday Trans.* **92**(10), 1793 (1996).
51. Aika, K., and Lunsford, J. H., *J. Phys. Chem.* **81**, 1393 (1977).
52. Aika, K., and Lunsford, J. H., *J. Phys. Chem.* **82**, 1794 (1978).
53. Takita, Y., and Lunsford, J. H., *J. Phys. Chem.* **83**, 683 (1979).
54. Takita, Y., Iwamoto, M., and Lunsford, J. H., *J. Phys. Chem.* **84**, 3079 (1980).
55. Iwamoto, M., and Lunsford, J. H., *J. Phys. Chem.* **84**, 1710 (1980).
56. Lin, C. H., Wang, J. X., and Lunsford, J. H., *J. Catal.* **111**, 302 (1988).
57. Iwamatsu, E., Moriyama, T., Takasaki, N., and Aika, K., *J. Catal.* **113**, 25 (1988).
58. Valentine, J. S., *Chem. Rev.* **73**, 237 (1973).
59. Smith, P., *J. Phys. Chem.* **60**, 1471 (1956).
60. Bielañski, A., and Haber, J., "Oxygen in Catalysis." Dekker, New York, 1991.